PERGAMON

Journal of Geodynamics 34 (2002) 405–445

JOURNAL OF
GEODYNAMICS

www.elsevier.com/locate/jog

# ICESat's laser measurements of polar ice, atmosphere, ocean, and land

H.J. Zwally[a,*], B. Schutz[b], W. Abdalati[c], J. Abshire[a], C. Bentley[d], A. Brenner[e], J. Bufton[a], J. Dezio[f], D. Hancock[a], D. Harding[a], T. Herring[g], B. Minster[h], K. Quinn[g], S. Palm[i], J. Spinhirne[a], R. Thomas[j]

[a]*Earth Sciences Directorate, Code 900, NASA Goddard Space Flight Center, Greenbelt, MD 20771, USA*
[b]*Center for Space Research, University of Texas, Austin, TX 78722, USA*
[c]*NASA Headquarters, Washington DC, USA*
[d]*Department of Geology and Geophysics, University of Wisconsin, Madison, WI, USA*
[e]*Raytheon ITSS, Code 971, NASA Goddard Space Flight Center, Greenbelt, MD 20771, USA*
[f]*ICESat Project Office, Code 425, NASA Goddard Space Flight Center, Greenbelt, MD 20771, USA*
[g]*Massachusetts Institute of Technology, Cambridge, MA 02139, USA*
[h]*Scripts Institute of Oceanography, University of California San Diego, La Jolla, CA 92093, USA*
[i]*SSAI, Code 912, NASA Goddard Space Flight Center, Greenbelt, MD 20771, USA*
[j]*EG&G, Inc, NASA Wallops Flight Facility, Wallops Island, VA 23337, USA*

**Abstract**

The Ice, Cloud and Land Elevation Satellite (ICESat) mission will measure changes in elevation of the Greenland and Antarctic ice sheets as part of NASA's Earth Observing System (EOS) of satellites. Time-series of elevation changes will enable determination of the present-day mass balance of the ice sheets, study of associations between observed ice changes and polar climate, and estimation of the present and future contributions of the ice sheets to global sea level rise. Other scientific objectives of ICESat include: global measurements of cloud heights and the vertical structure of clouds and aerosols; precise measurements of land topography and vegetation canopy heights; and measurements of sea ice roughness, sea ice thickness, ocean surface elevations, and surface reflectivity. The Geoscience Laser Altimeter System (GLAS) on ICESat has a 1064 nm laser channel for surface altimetry and dense cloud heights and a 532 nm lidar channel for the vertical distribution of clouds and aerosols. The predicted accuracy for the surface-elevation measurements is 15 cm, averaged over 60 m diameter laser footprints spaced at 172 m along-track. The orbital altitude will be around 600 km at an inclination of 94° with a 183-day repeat pattern. The on-board GPS receiver will enable radial orbit determinations to better than 5 cm, and star-trackers will enable footprints to be located to 6 m horizontally. The spacecraft attitude will be controlled to point

* Corresponding author.
*E-mail address:* zwally@icesatz.gsfc.nasa.gov (H.J. Zwally).

0264-3707/02/$ - see front matter 
PII: S0264-3707(02)00042-X

the laser beam to within ±35 m of reference surface tracks at high latitudes. ICESat is designed to operate for 3–5 years and should be followed by successive missions to measure ice changes for at least 15 years.


## 1. Introduction

The huge ice sheets of Greenland and Antarctica hold enough fresh water to raise global sea level by 80 m if they melted completely. Although major melting is not imminent, the ice sheets change continually in response to natural processes and are expected to respond to greenhouse-induced climate warming as well. The annual mass exchange between the ice sheets and the ocean is about 8 mm/year of global sea level equivalent, so even small changes in this rate of mass exchange are significant. Moreover, some parts of the ice sheets may be more susceptible to rapid changes. The West Antarctic Ice Sheet alone contains the equivalent of 6–7 m of sea level rise and rests on a bed far below sea level, a configuration that may make it susceptible to dynamic instabilities (Bindschadler, 1998; Oppenheimer, 1998; Bentley, 1997). The Greenland ice sheet is only about 1/8 as large as the Antarctic ice sheet but may be more vulnerable to climate warming because summer melting already occurs over much of its surface.

The 1992 IPCC (Intergovernment Panel on Climate Change) Supplement on Scientific Assessment of Climate Change noted that the largest uncertainty about sea level is "rooted in our inadequate understanding of polar ice sheets whose response to climate change also affects predictions of sea level rise" (Houghton et al., 1992). The National Academy of Sciences (1990) stated "possible changes in the mass balance of the Greenland and Antarctic ice sheets are fundamental gaps in our understanding and are crucial to the quantification and refinement of sea-level forecasts." This uncertainty was further iterated by Fitzharris et al. (1996), who noted "monitoring of key components of the cryosphere must continue. The mass balance of the ice sheets of the world is poorly known." Although sea level changes in response to input from ice caps and glaciers, as well as thermal expansion of the ocean itself, the ice sheets contain the potential for the most significant contribution to sea level rise simply because they contain so much ice. The impact of even small rises in sea level has been widely studied. Aside from the threat of inundation faced by low-lying coastal areas, increased beach erosion that would occur before inundation, for example, is a serious economic concern (Yohe and Schlesinger, 1998; Neumann et al., 2000).

The primary purpose of ICESat (Fig. 1.1 and http://icesat.gsfc.nasa.gov/) is the determination of inter-annual and long-term changes in polar ice-sheet mass, the causes of changes in mass balance (polar precipitation, ice melting, or ice flow acceleration/deceleration), and the impact of these changes on global sea level. Changes in ice mass (Fig. 1.2) are caused by an imbalance between the ice mass inputs (snowfall, condensation, and occasional rainfall) and outputs (evaporation, melt runoff, iceberg discharge, and snow drift removal). Conventional methods of studying ice sheet mass balance examine the difference between the mass input and output terms, but significant errors in these quantities have limited determinations to about ±25% (Warrick et al., 1996), which is equivalent to ±2 mm/year of sea level change. Measurements of sea level from the TOPEX/POSEIDON radar altimeter show a current rise of +2.1±1.3 mm/year (Nerem et al., 1997), which is comparable to the rise over the last century measured by tide gauges (Warrick et al., 1996; Douglas, 1997).


Fig. 1.1. ICESat will carry the Geoscience Laser Altimeter System (GLAS) for measurement of changes in the size of Earth's polar ice sheets, the heights of global clouds and aerosols, and global land topography.

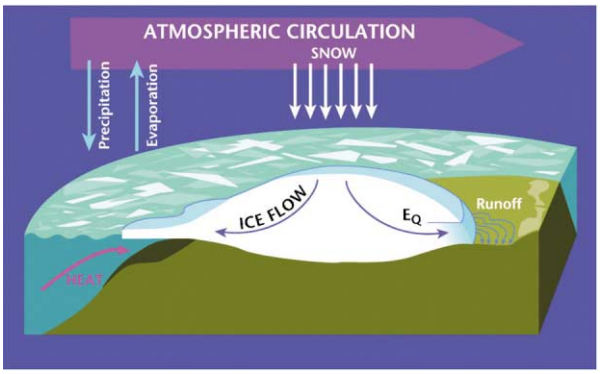


Fig. 1.2. Snow accumulation on the polar ice sheets is approximately balanced by ice flow toward the margins where the ice below the equilibrium line (EQ) melts or calves into icebergs. Changes in the annual water exchange of about 8 mm of global sea level can be caused by changes in the atmospheric/ocean temperatures or circulations or by internal changes in the ice dynamics. A 1 m change in the average ice-sheet thickness of 2360 m would cause a global sea level change of about 4 cm.

The concept of using satellite-altimeters to measure ice elevation changes and determine ice-sheet mass balance (Zwally, 1975) is based on the simple relationship of ice surface elevation changes to changes in ice thickness and therefore ice mass. Surface elevation changes are equivalent to ice thickness changes minus the vertical motion of the bedrock, which is generally smaller and can be separately estimated. In addition, short-term changes caused by variations in rates of near-surface firn compaction must be accounted for (Arthern and Wingham, 1998; Zwally and Li, 2002). Despite the limitations of ocean radar altimeters over the sloping surfaces on ice sheets, elevation changes from radar altimeter measurements that are indicative of changes in ice mass balance have been reported (e.g. Zwally, 1989; Davis et al., 1998; Wingham et al., 1998; Zwally and Brenner, 2001). In 1979, satellite laser altimetry was proposed (Campbell et al., 1979) for measurement of ice sheet elevation changes, because of the advantages of the smaller laser footprint and the restriction of laser reflections to a small surface layer.

Prediction of sea level rise during the next century requires not only an assessment of the current rates of mass gain or loss of the Greenland and Antarctic ice sheets, but information on how the ice balance changes with changes in polar precipitation, temperature, cloudiness, and perhaps other factors. All of these factors, including the ice sheet surface mass balance processes, undergo interannual and decadal variations as well as longer term changes. Therefore, ICESat should be followed by successive missions to measure ice changes continuously for at least 15 years.

In atmospheric science, incomplete knowledge of clouds and aerosols causes one of the main uncertainties in modeling and prediction of global climate warming. Climate is especially influenced by the vertical structure and horizontal coverage of clouds, which alter the radiative fluxes at the top and bottom of the atmosphere and determine the vertical distribution of atmospheric heating rates. In particular, direct knowledge of cloud heights has been a limiting factor. In addition, while the climatic effect of increasing $CO_2$ and other greenhouse gases is well known, a concurrent increase in anthropogenic aerosols is believed to have an opposite cooling effect (Trenberth et al., 1996). Aerosols affect the earth's energy budget and climate by scattering and absorbing radiation (direct effect) and altering cloud particle size and number density, which ultimately affect the cloud albedo, scattering, and absorption properties (indirect effect). The exact magnitude of the aerosol cooling is unknown, but is thought to offset a substantial fraction of the greenhouse warming. A major reason for the uncertainty has been the limited ability to make global observations of tropospheric aerosols, especially over land.

ICESat will provide continuous global measurements of vertical cloud and aerosol structure and optical depth, planetary boundary layer height, and polar tropospheric and stratospheric clouds for the first time. The direct and unambiguous lidar data will also be used for validation of the cloud and aerosol retrievals from the passive sensors on other EOS satellites. Passive sensors view cloud tops very well, but the presence of upper layer clouds limits their ability to distinguish multi-level cloud formations and to determine the vertical distribution of clouds. Unique aspects of ICESat's lidar are the direct measurements of cloud heights, monitoring of aerosol distributions over land, and all-year measurements of clouds and aerosols in polar regions. In polar regions, improved measurements of clouds is especially important for understanding the radiation balance and for improving the atmospheric modeling of precipitation, both of which directly affect the surface ice mass balance.

The land topographic measurements of ICESat will provide a network of high-accuracy profiles along the 183-day repeat tracks with a maximum cross-track separation of 15 km at the equator. These observations will improve digital elevation models where geodetic control is scarce, particularly in the higher-latitude regions. Repeat laser profiling and crossover analysis may be used to detect changes in land elevation caused by geologic processes such as soil erosion, sediment transport, and magma inflation of volcanoes. Changes in inland water levels can also be monitored and vegetation height can be measured in low-relief areas. An important feature of ICESat is the capability to accurately point the spacecraft to off-nadir targets of opportunity, such as volcanic aerosol plumes or regions inundated by floods.

ICESat measurements (Fig. 1.3) will be made by the Geoscience Laser Altimeter System (GLAS), which utilizes 1064-nm laser pulses for measuring the heights of the surface and dense cloud and 532 nm pulses for measuring the vertical distribution of clouds and aerosols. Laser footprints with 60 m diameter and 172 m along-track spacing will have a surface-ranging accuracy of 10 cm. ICESat's orbital altitude will be 600 km at an inclination of 94° with a 183-day

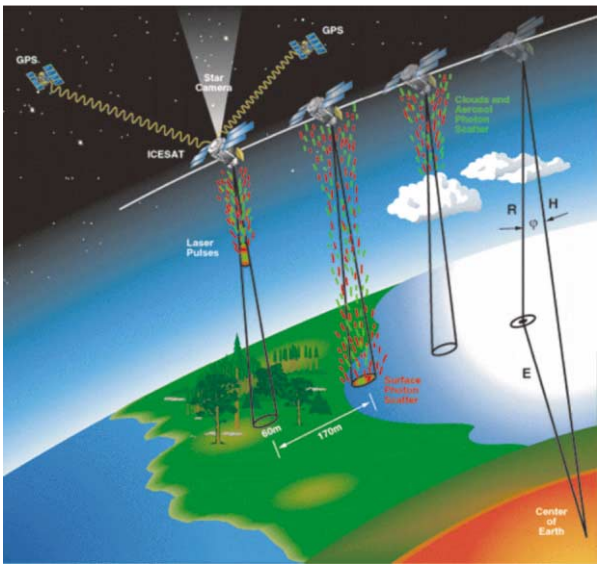


Fig. 1.3. The GLAS instrument on ICESat measures ranges to the surface and to clouds and aerosols in the atmosphere using short laser pulses at two frequencies (near infrared and green). The satellite position is determined using signals from the Global Positioning System of satellites. ICESat's orientation, the angle of the laser beam, and the location of the laser footprint on the surface are determined by a star-tracking and beam-attitude measurement system in GLAS.

repeat pattern. The on-board GPS system will enable radial orbit determinations to better than 5 cm, and star-trackers in GLAS and on the spacecraft will enable footprints to be located to 6 m horizontally. Spacecraft pointing of the laser beam can be controlled to within $\pm 35$ m on the surface for precise control of repeat tracks over the ice sheets.

The ICESat spacecraft and GLAS instrumentation are designed to operate continuously for at least 3 years with a goal of 5 years. Full-scale development of GLAS began in May of 1997 at NASA's Goddard Space Flight Center, and Ball Aerospace Corporation contracted to build the ICESat spacecraft in February 1998. The launch of ICESat on a Boeing Delta-2 rocket from Vandenberg, California is planned for December 2002, along with a second smaller payload, the Cosmic Hot Interstellar Plasma Spectrometer Satellite (CHIPS).

## 2. Ice sheet science

Antarctica straddles the South pole and has a dominant influence on its own climate, and on the surrounding ocean. Surface melting during summer is mostly restricted to peripheral ice shelves and some near coast parts of the ice sheet (Zwally and Fiegles, 1994). Away from the coast, much of Antarctica is a cold desert with very low precipitation rates. Ice drainage is primarily through outlet glaciers and ice streams, some of which penetrate deep into the heart of the ice sheet moving at speeds of a few hundred meters per year to over 1 km/year in some cases. Many glaciers and ice streams converge into floating ice shelves, which are also fed by snow accumulation on their surfaces. Thus, ice loss from the Antarctic ice sheet is primarily through

the ice shelves by basal melting and iceberg calving at the ice fronts. The ice shelves thin towards their seaward ice fronts, partly by ice creep and partly by basal melting at rates generally of a few tens of cm/year. Although mass changes in the floating ice shelves have no direct effect on sea level, changes in the ice shelves could alter their buttressing effects on the ice streams and their rates of discharge from the ice sheets.

By contrast, the Greenland climate is strongly affected by its proximity to other land masses and to the North Atlantic, with the warm Gulf Stream to the south and regions of North Atlantic deep water production to the east and west. Summer melting occurs over about 20% of the ice-sheet surface (Abdalati and Steffen, 1997), depending on summer temperatures, with most of the resulting melt water flowing into the sea. The average accumulation rate in the accumulation zone is about 26 cm water/year, compared to 16 cm water/year for Antarctica. The zone of net ablation, which is about 9% of the total Greenland ice sheet, has an average annual net mass loss of 126 cm water/year. Although the Greenland ice sheet is smaller, its total annual exchange of water with the ocean is about 25% as large as for Antarctica. Ice-core data from the summit of the Greenland ice sheet indicate that Greenland temperatures and accumulation rates can change significantly over periods of a few years to decades (Alley et al., 1993).

Ice sheets thicken by snow accumulation and thin by snow densification, ice creep and motion, and evaporation and melting. Rates of snowfall, evaporation, densification, and melting change significantly throughout the year and from one year to the next; ice creep and ice motion exhibit only small changes on sub-decadal time scales. Consequently, the ice surface rises and falls in response to the seasonal and interannual changes. The magnitude of this short-term elevation variability is poorly known, but is estimated to be on the order of tens of cm to a meter over the accumulation zones of Greenland and Antarctica. Near the coasts, where snow accumulation and melt rates are higher, this short-term variability may increase to a few meters. These short-term changes must be monitored for two major reasons: to infer the interannual variability of snow-accumulation and melting rates, and to reveal the longer-term changes in ice-sheet volume that could seriously affect sea level.

Ice sheets are actually complex composites of individual drainage systems or basins, some of which are characterized by fast-moving low-gradient ice streams bordered by slowly flowing ice, some by huge outlet glaciers through peripheral mountain ranges, and others by broad expanses of open sheet flow with only small, local glaciers. Estimated thickening/thinning rates tend to be small (e.g. $<0.1$ m/year) over the accumulation regions, and considerably larger (several tenths to more than 1 m/year) over the ice streams and seaward margins. Thickening or thinning trends will undoubtedly be different for each major ice drainage basin. The dynamic behavior of a particular drainage system may be nearly independent of the dynamic behavior of its neighbors, and variations in the surface mass balance, as may be driven by changes in atmospheric circulation and storm tracks, can differ from basin to basin. Consequently, elevation changes must be measured over all the major drainage basins, and in enough spatial detail to detect major redistributions of volume within each basin. Details of the mass redistribution will help explain whether the changes are caused by long-term dynamical effects on the ice flow or by shorter-term climatic effects on the surface mass balance.

Based on very recent results, the Greenland ice sheet has a negative net balance, contributing almost 10% to the total observed sea-level rise (Krabill et al., 2000). Taken as a whole, the higher-elevation parts of the ice sheet are close to balance (Thomas et al., 2000a; Davis et al,

2000), but there is significant near-coastal thinning (Krabill et al., 2000; Abdalati et al., in press), at rates up to 10 m/yr on one major outlet glacier (Thomas et al., 2000b). The results at higher elevations are from three independent analyses, using satellite radar-altimeter data (only south of 72° N), aircraft laser-altimeter data, and comparison of total ice discharge with total surface accumulation. However, the assessment of near-coastal thinning was possible only by the airborne laser-altimeter measurements. While the airborne laser system provides accurate change measurements in the lower-elevation margins of the ice sheets (where radar altimetry is limited by the surface slopes and undulations), the airborne measurements are limited in their spatial and temporal coverage. Usually survey flights are made only in the late-spring/early summer at intervals of about 5 years. Therefore, the measured changes are necessarily characteristic of summer-to-summer trends and may be biased by undetected interannual variability. For example, Bromwich et al. (2001) shows increases in precipitation over the interior of the ice sheet north of 70° N in the mid to late 1990′s that might not have been captured in the airborne-measured elevation changes. This highlights the importance of monitoring future behavior of Greenland regions with ICESat data, and of making similar surveys over the Antarctic ice sheet where aircraft surveys are not practical.

The objective of ICESat is to measure profiles of ice sheet surface elevation with sufficient accuracy, spatial density, and temporal coverage so that inter-annual and long-term elevation changes can be derived with an accuracy of $<1.5$ cm/year for spatial-averages of measurements over areas of $100\times100$ km on the ice sheets. The spatial scale is required to resolve details of the basin scale mass redistribution and the effects of changes in major ice streams and outlet glaciers. The vertical resolution is required to resolve changes that are about 10% of the accumulation rate as a typical value. In regions where the accumulation is higher than average, a lesser resolution would be acceptable, whereas in some interior low accumulation regions a larger spatial averaging will be used to achieve a better than 1.5 cm/year accuracy.

The elevation profiles will consist of the mean elevations over the 60 m laser footprints, with an elevation accuracy of 15 cm, spaced at 172 m along-track as described in other sections. The pattern of ICESat ground tracks over the margin of west-central Greenland is shown in Fig. 2.1. Surface elevation changes are usually calculated at crossovers between successive ascending and descending passes over the same location (a crossover point), by interpolation between successive footprints. Analysis of the error caused by interpolation has been estimated with aircraft laser data to be less than several cm over most of the ice sheets where the surface undulations between footprints are small. Spatial averages of elevation changes are obtained by averaging the elevation differences at a set of crossovers in a chosen area, typically 50 by 50 km or larger, taking into account the varying time intervals between the measurements. For random errors, approximately 100 crossover differences are required to reduce the error on the mean elevation change to 1.5 cm. Over most of the ice sheets, the number of available crossovers should be sufficient to achieve $<1.5$ cm/year over $100\times100$ km areas, using the conservative assumption of 50% loss due to cloud cover (i.e. 75% crossover loss). Furthermore, in addition to differences at crossovers, considerably more elevation differences will be obtained from analysis of the precise-repeat track profiles that will be maintained to within $\pm35$ m cross-track.

Time-series of surface elevations, $H(t)$, having sufficient resolution to show seasonal changes are created by the sequence of average crossover differences between the first 90-day interval and each of the successive 90-day intervals, combined with the sequence from the second interval

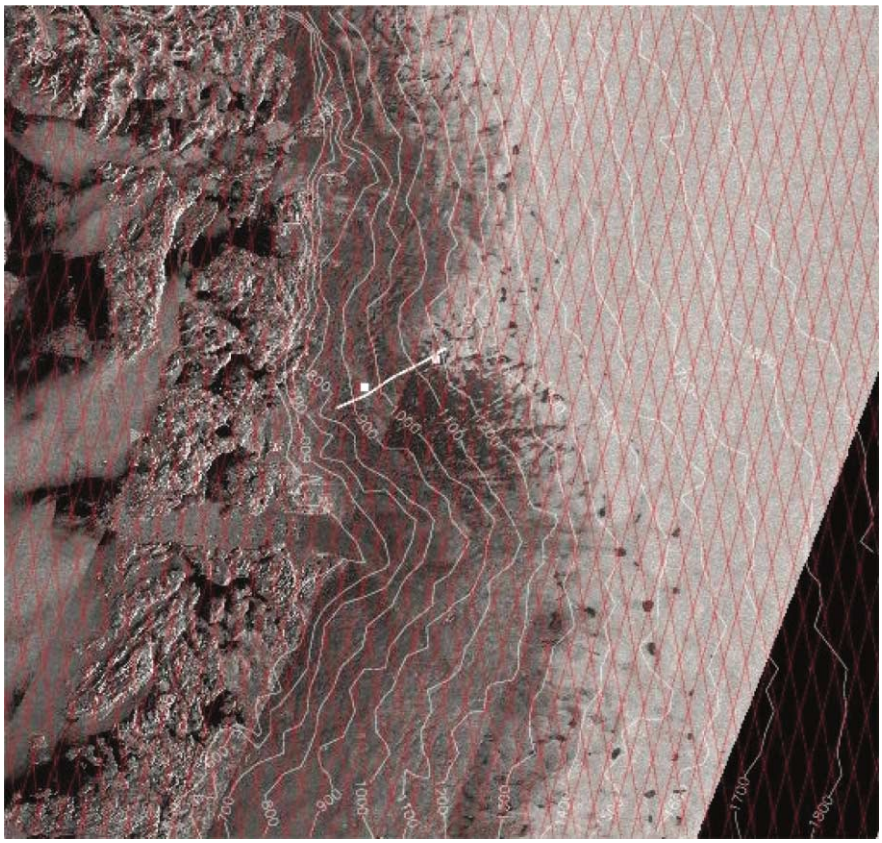

Fig. 2.1. ICESat ground tracks for 183-day repeat cycle overlain on a SAR image (195 km N–S by 205 km E–W) of the ice margin in west-central Greenland along with surface elevation contours (100 m intervals) mapped from ERS radar altimeter data. Location of the U. of Colorado's Swiss Camp (69° 34.3′ N, 49° 18.2′ W) on the equilibrium line at 1170 m elevation is shown in the center. The bare ice in the ablation zone is darker than the firn above the equilibrium line where darker summer-melt lakes are also visible.

crossed with each successive interval, and so forth for the sequences for the third and greater intervals (Zwally and Brenner, 2001). As the length of the measurement period increases, the number of crossovers for analysis increases in proportion to time squared. For an average of $M$ crossovers in each interval for $N$ time intervals, the total number of crossovers in the series for the first sequence from crossovers with the first interval is $N \times M$. However, the total number of crossovers in the combined $H(t)$ series for all sequence is $M \times \Sigma_1^N (n) = M \times N(N+1)/2$, which is $(N+1)/2$ times larger. In addition to the traditional crossover differences, elevation differences from the precise-repeat track profiles can be included in the time series in a similar manner. The $H(t)$ time series is then analyzed to infer the character of the changes, for example, a seasonal cycle imposed on a linear trend.

$H(t)$ time series constructed from crossovers from 7 years of ERS-1 and ERS-2 data at two locations in West Antarctica, are shown in Fig. 2.2. In each case, crossovers within a 100 km radius and $\pm 250$ m elevation of the reference point are included. The data are corrected for an

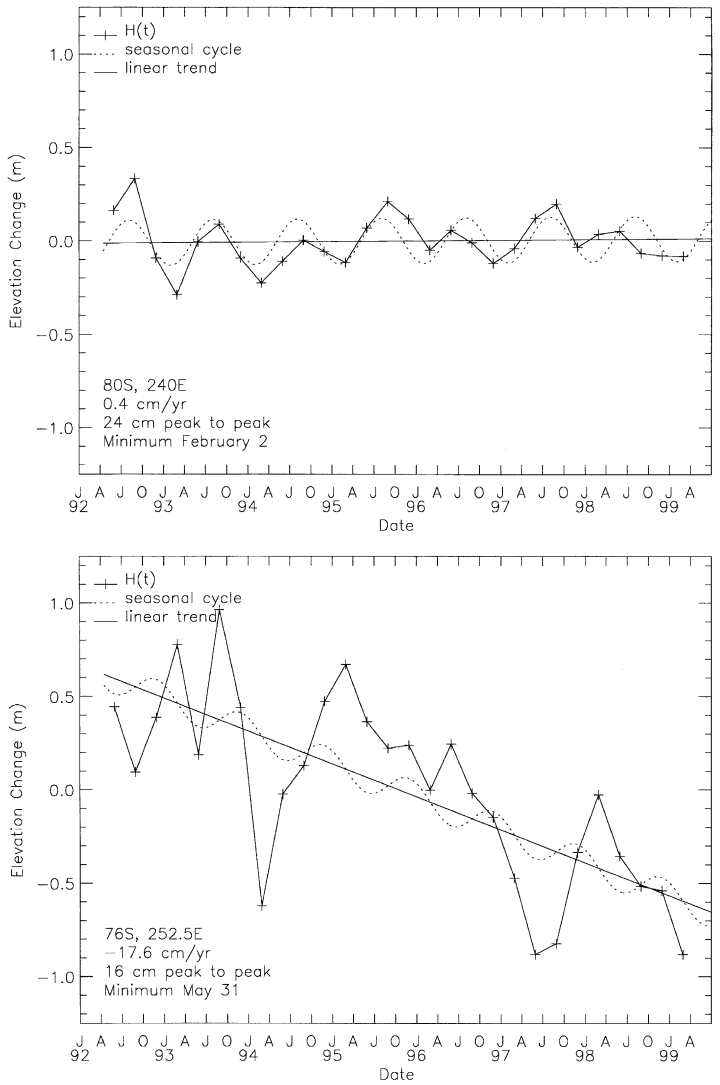


Fig. 2.2. *H(t)* series for 2 locations in West Antarctica showing a near-zero elevation change near Byrd Station (top) and a thinning of 17.6 cm/year inland of Thwaites Glacier (bottom). Seasonal amplitude is largely due to variations in the rate of firn compaction with the minimum in March following the warmer summer temperatures. Time series is constructed from sets of crossover averages between successive 90-day intervals using crossovers within 100 km radius and ±250 m elevation of the location.

unexpected inter-satellite bias that was determined by Brenner et al. (2000) from analysis of crossover differences acquired during the 12 months of overlapping operation of ERS-1 and ERS-2. The bias was found to vary with received backscatter power, which depends on the surface slope and therefore varies with elevation. In this region, the bias lowers the ERS-2 elevations relative to ERS-1 by 17.4 cm at 500 m elevation and 11 cm at 2000 m. Corrections are also made for variations in the derived ranges with changes in the backscatteed power, similar to those made by Wingham et al. (1988).

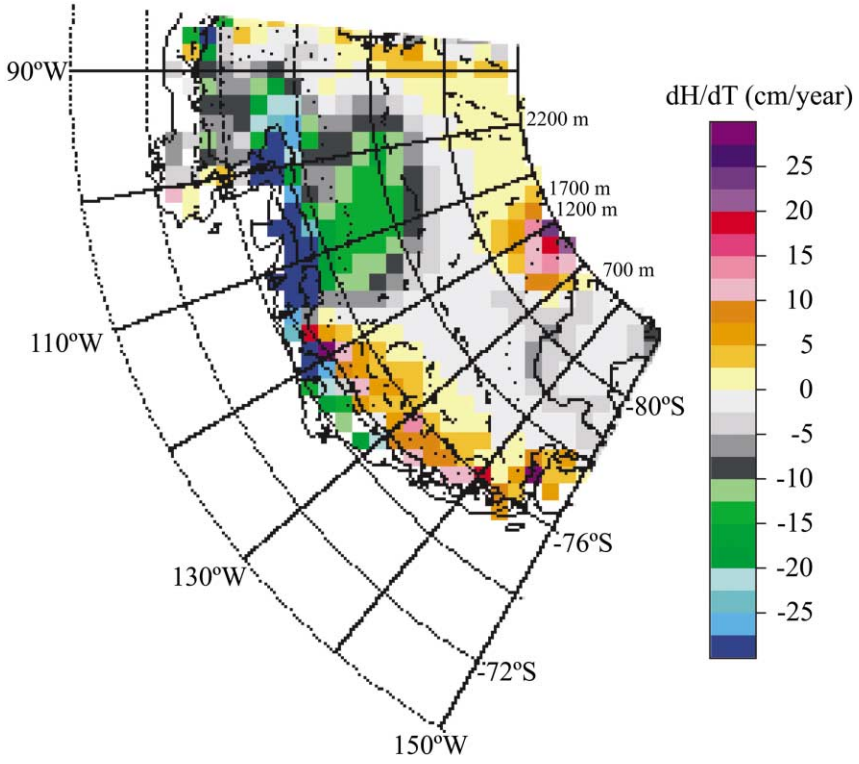


Fig. 2.3. Elevation change map of a portion of the West Antarctic ice sheet showing up to −30 cm/year thinning in the Pine Island/Thwaites drainage basin in the Northeast and up to 20 cm/year thickening on the ridge between the Pine Island/Thwaites Glacier and the Ross Ice-Shelf drainage basin in the western part. d$H$/d$t$ values mapped on 50 km grid are from multi-variate linear and sinusoidal fits to $H(t)$ time series of elevation differences at crossovers within 100 km radius and ±250 m elevation of the grid center.

The first $H(t)$ series, which is centered at Byrd Station (80° S, 120° W) at 1526 m, shows a near-zero change of 0.4±1.0 cm/year and a peak-to-peak seasonal amplitude of 24 cm. The second location (76° S, 107.5° W) at 893 m elevation about 100 km inland of the Thwaites Glacier tongue has a significant thinning of −17.6±3.5 cm/year, with smaller and irregular seasonal amplitude of 16 cm. For the ice sheet summit (72.57° N, 38.45° W) in Greenland, a fitted seasonal amplitude of 25 cm with more interannual variability than at Byrd was modeled (Zwally and Li, 2002) using a temperature-dependent rate of firn compaction and the observed seasonal and interannual variations in temperature from automatic-weather-station data (K. Steffen, pers. com.). Most of the annual compaction of the upper layers of firn occurs during the warmer summer months, as illustrated by the February minimum in the seasonal cycle at Byrd Station in Fig. 2.2.

Previously, Wingham et al. (1998) reported a −11.7±1.0 cm/year thinning trend averaged over the Pine Island Glacier and Thwaites Glacier drainage basins for the period 1992–1996, also from ERS data. This region is of particular interest, because Pine Island and Thwaites Glaciers drain a large part of the West Antarctic ice sheet and may be undergoing significant changes (Vaughan et al., 2001). For example, recent analysis of ERS SAR interferometry showed the position of the hinge line of the Pine Island glacier retreated 1.2 km/year in the same period as the altimeter

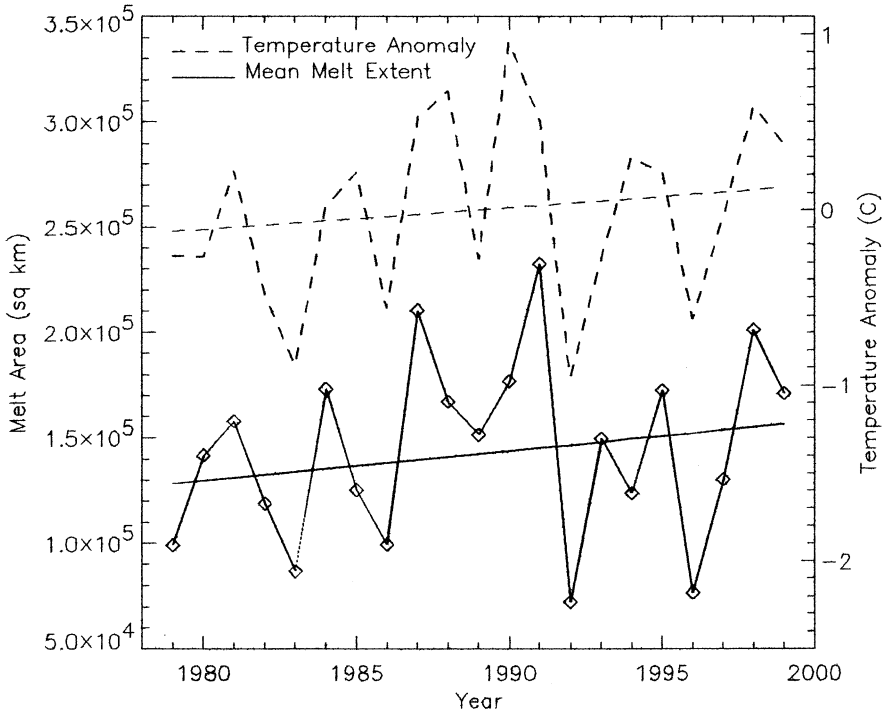


Fig. 2.4. Mean extent of surface melting on the Greenland ice sheet and average temperature anomalies at six coastal stations for 1979–1999. The increasing trend in melt extent is 0.97%/year while the temperatures warmed 0.24/C over the 21-year period. (Melt-temperature correlation coefficient is 0.82.) Melt measurements are from long-term satellite passive- microwave sensing.

measurements of elevation change (Rignot, 1998). In the region from 85° to 150° W, the elevation changes range from about −30 cm/year to +20 cm/year, as shown in the map of $dH/dt$ in Fig. 2.3. The $dH/dt$ increases are at higher elevations on the ridge between the Pine Island and the Ross-Ice Shelf drainage basins. The average elevation change for the grounded ice (excluding the floating ice shelves) is −4.3 cm/year. Using an estimate of 2.5 cm/year for the average rate of bedrock uplift (cf. Huybrechts and Le Meur, 1999), gives an average ice-thinning rate of 6.8 cm/year and a mass loss of 67 Gt/year, and a contribution to sea level rise of 0.2 mm/year for this part of West Antarctica.

During 3–5 years of ICESat-1 operation, an estimate of the overall ice sheet mass balance and sea level contribution during the period of measurements will be obtained. One estimate of the accuracy of a linear trend deduced from ICESat data over 5 years for all of Antarctica is ~7 mm/year of water equivalent, including errors in the estimates of firn compaction and post glacial rebound (Wahr et al., 2000). Their estimate of the accuracy for deducing long-term trends was 9 mm/year, obtained by including the difference between a typical 5-year and century-scale trends from simulations of variations in Antarctic precipitation.

Currently, correction for post-glacial rebound is made using coupled models of ice sheet evolution and the visco-elastic response of the solid Earth (Huybrechts and Le Meur, 1999). In the future, however, estimates of the basal motion can be improved (Wahr et al., 2000) through the

combined analysis of data from ICESat and the Gravity Recovery and Climate Experiment (GRACE) missions, which are expected to fly concurrently. Gravity measurements are sensitive to changes in mass under the satellite, including mass redistribution due to crustal uplift and mantle inflow and changes in the mass of snow and ice in the ice sheet. For a given mass change, the surface height changes would be in the ratio of 1–3.5–10, respectively, for isostatic uplift, changes in solid ice, and changes in snow accumulation at the surface because of their different mass densities. Therefore, measurements of both change in height and change in gravity make it possible to improve the post-glacial rebound estimates, with an accuracy that improves with the length of concurrent measurements.

Continued ice-elevation change measurements after the first ICESat are important to determine the variability in mass balance and sensitivity to climate change. For example, the variability in the area of Greenland surface melt observed from satellite passive microwave data over 17-years and its correlation with temperature is shown in Fig. 2.4. Whereas the passive microwave only provides the area of surface melting, ICESat's elevation changes will provide the volume of melt water produced from the marginal ablation zones. While rates of ice flow in the ice sheets change only slightly on decadal time scales, the surface mass balance and mass exchanges with the atmosphere and ocean change instantaneously with changes in precipitation and melting. For the purpose of understanding and predicting changes in ice mass and sea level, observation over decadal time scales is essential. ICESat data on seasonal and inter-annual changes in surface elevation will provide unique information for validation of atmospheric models of precipitation-evaporation in polar regions, as well as energy-balance models of surface melting and snow accumulation on the ice sheets.

## 3. Atmospheric science

The value of direct measurements of the height distribution of clouds and aerosol in the atmosphere by a satellite lidar has been recognized for over 20 years (Curran, 1989). Current satellite and other data provide considerable information on cloud and aerosol distributions (e.g. Rossow and Cairns, 1995). However, some critical parameters can only be obtained by active optical profiling. Specifically, passive techniques can not resolve the height profile of aerosols, which is required for modeling aerosol transport and height-resolved radiative heating/cooling effects. For transmissive and multi-layer clouds, passive techniques are limited in accuracy. The ICESat GLAS active lidar profiling will supplement passive cloud sensing with data to vertically resolve the heating and cooling effects of global cloud cover and aerosols.

The concept of the GLAS atmospheric lidar measurements as a combined measurement with laser surface altimeter is based on the fundamental compatibility of basic instrument requirements. Although atmospheric signals are typically much smaller than for the surface echo signals, the vertical resolution requirement is much less, because 75 m is sufficient for almost all requirements. As is well known, the signal to noise of measurements increases with decreasing bandwidth or resolution. Thus, there is a compatibility between the required product of laser power and telescope aperture for precision surface altimetry and basic profiling of clouds and aerosols. Therefore, the cost of a space mission to obtain both observations is significantly less than for two separate experiments.

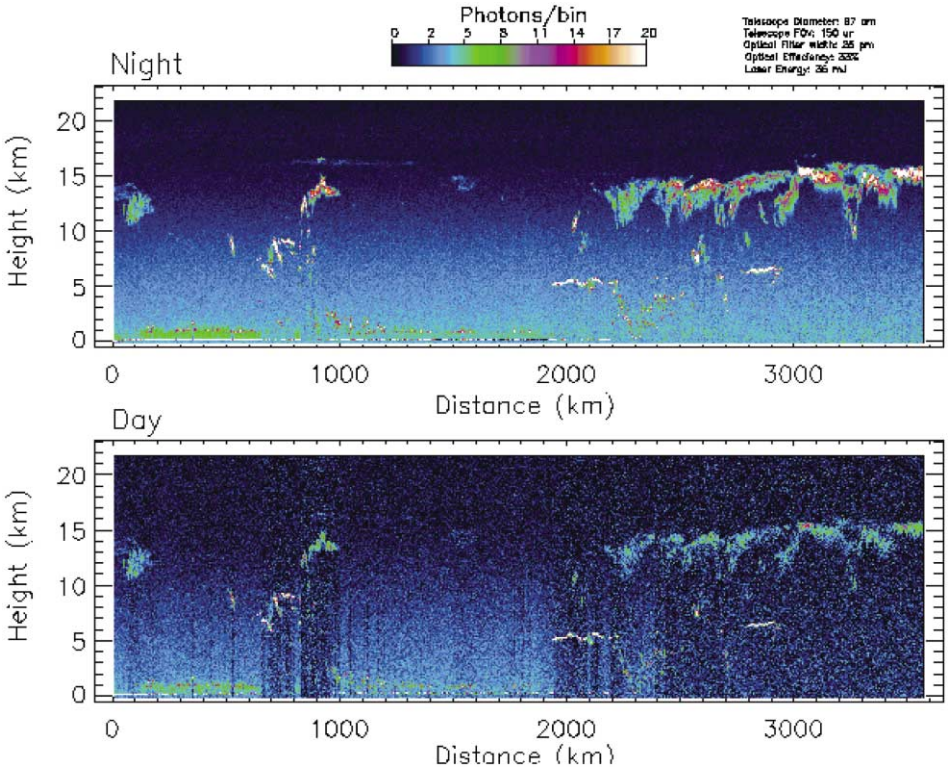


Fig. 3.1. A nighttime (upper) and daytime (lower) simulation of the GLAS 532 nm signal using aircraft lidar data acquired during the TOGA-COARE experiment. Color coding represents the expected received signal in photons per height bin (76.8 m/bin). The simulation parameters are: 96 cm telescope diameter, 150 μrad field of view, 36 mJ laser energy, 0.025 nm filter width, 60% detector quantum efficiency, and 33% total optical transmission.

### *3.1. Atmospheric measurement objectives*

The ICESat atmospheric science objectives are to measure cloud heights and vertical profiles, polar clouds, aerosol profiles, and planetary-boundary-layer heights. The GLAS measurement of cloud heights and vertical profiles are described in detail in Spinhirne and Palm (1996). The laser measurements will provide an image of the vertical structure, or morphology of cloud systems as shown in Fig. 3.1 using aircraft data adjusted to simulate GLAS data. Such morphology information has applications for studies of cloud and storm formation processes. As an example, recent studies indicate that many thick-cirrus clouds form primarily from precipitation by very-thin generating layers. The layers and their precise height can be clearly determined from the structure revealed by the laser profiles. The correlation of generating layers with temperature and humidity fields will aid in the parameterization of cirrus formation processes. Combined with passive measurements of clouds, the active measurements will significantly enhance progress on determining the 4-D distribution of cloud optical properties and the relationships between these properties and cloud liquid water, ice mass, and water vapor.

Optically thin, or sub-visual, cirrus clouds are potentially a significant greenhouse component of the atmosphere (Jensen et al., 1996). Recent measurements indicate that over 50% of the warm-pool region in the Western Pacific is typically covered by a sub-visible layer of cirrus at the tropopause. Although the optical thickness of this layer is small, the net radiative impact over the entire region is estimated to be significant. Reliable detection and appropriate sampling is not possible by passive means. The GLAS lidar will provide a very sensitive measure of the presence, height and thickness of tenuous cirrus layers.

A major goal is to observe multiple-layered and broken-cloud cover, as well as the height of the cloud tops. For a large fraction of cloud cover, GLAS will detect the cloud-base height. Cloud effects on surface warming are largely related to the cloud component of the downward atmospheric flux. A principal determining factor of the cloud flux component is the distribution of cloud-base heights. For clouds forming in the planetary boundary layer (PBL), the cloud base indicates the lifting condensation level (LCL). The LCL is a significant variable for boundary layer dynamics. From the LCL, the near surface moisture over the oceans can be accurately derived (Palm et al., 1998).

Polar cloud observations will have special value, because passive techniques are limited by darkness part of the year and cold temperatures and bright backgrounds (snow and ice) the rest of the year. GLAS measurements will unambiguously define cloud type and fraction, which define the net radiation balance of the Arctic regions and strongly affect atmospheric dynamics. In the cold seasons in the Arctic, hazes of small ice crystals, or diamond dust, occur in the lower troposphere greatly reducing visibility. The ice crystals are an important factor in the radiation transfer, which determines the vertical temperature and humidity structure of the winter Arctic atmosphere. For studies of ice sheet mass balance, cloudless ice-crystal precipitation is believed to be a dominant source of precipitation in large areas of Antarctica. GLAS active laser sensing will give the first spatial and temporal distribution of clouds and diamond dust for polar precipitation.

Aerosol profiles provided by the GLAS instrument will uniquely define the vertical aerosol structure throughout the troposphere over land and ocean. Vertically-elevated layers of particulates are transported over long ranges and have been linked to major climate and atmospheric-chemistry impacts. Also, transported aerosols are thought to influence air quality and ocean nutrients. Ground-based lidar measurements have long been a standard for monitoring volcanic aerosol layers in the stratosphere. The ICESat measurements will give global coverage of episodic aerosol events such as volcanic emissions, biomass burning, ablated desert soils, continental particulates, and arctic haze. When coupled with wind direction and speed, the vertical distribution of aerosol trace materials provides information on aerosol mass transport. Long-range transport of trace gases and aerosols is a dominating factor in the global chemical balance, for which accurate aerosol vertical-profile information is required.

The height of the PLB is a basic parameter linking the surface to atmosphere dynamics, especially over the world oceans. However, there is currently no way to obtain accurate PBL height measurements on a global basis. GLAS observations will determine the heights of cloud-capped boundary layers with high accuracy. In many areas, GLAS observations will also determine the height of the mixed layer from the aerosol scattering structure. Global observations of the PBL height will be very important for verification of models and the study of PBL parameterizations.

The GLAS signal is sufficient to penetrate a large fraction of clouds and obtain a surface echo for an elevation measurement. Current data on polar cloud cover indicates that the optical thickness is sufficiently low for a surface laser signal to be obtained from some ice sheet areas

when classified as cloud covered. In conditions of partial transmission through clouds, small-angle scattering of photons from cloud particles will cause some photons to take a longer path length while still remaining within the GLAS field-of-view. The signal for the delayed photons appears later in the received waveform and the consequent asymmetric waveform affects the range accuracy (Duda et al., 2000), depending on the waveform fitting procedure discussed in Section 7. Although the delays of individual photons can be meters in range, the net effect on the derived range accuracy is typically at the centimeter level. Scattering from cirrus clouds in particular is highly forward peaked, and may affect a significant fraction of the scattered photons. However, the consequent delay is less for high clouds than for low-level clouds, because most of the multiply scattered photons will exit the field of view before striking the ground. The identification of surface echos that are influenced by clouds will be provided directly by the lidar channel. In principal, range corrections for forward scattering could be calculated if sufficient information on the cloud scattering is available.

### *3.2. Atmospheric measurement capabilities*

GLAS will measure the vertical structure of cloud and aerosol with sufficient vertical and horizontal resolution to resolve large-scale dynamically and energetically important variability. Sufficient accuracy is needed for the optical thickness and vertical profile of total cross section to be obtained up to a limit of approximately 2–3 in optical depth. The vertical structure will be measured over the entire orbit including sunlit and dark scenes. The parameters needed from the GLAS observations are the height of boundaries and variables which relate to the radiation and other influence of clouds and aerosols. The basic parameter that defines the integrated-radiative influence of a layer is optical thickness. For vertical resolution of radiative forcing, the total extinction cross section (absorption plus scattering) is needed. Both the extinction cross section and optical thickness are derived parameters, which involve the height resolved laser scattering data and appropriate retrieval algorithms. For boundary layer and LCL height levels, the heights are derived values from analysis of the aerosol and cloud scattering structure.

In order to fulfill the science requirements, GLAS must measure the atmospheric scattered signal at the accuracies and spatial scales given in Table 3.2. These values are based on a complex analysis and extensive experience with aircraft lidar remote sensing (Spinhirne and Palm, 1996). The obtainable measurement accuracy and horizontal and vertical resolutions depend upon the instrument configuration and the atmospheric scattering cross sections. In essence, both horizontal and vertical averaging of data is available to make a given measurement when atmospheric cross sections are $10^{-4}$ (m-sr)$^{-1}$ or smaller.

Table 3.2
Atmospheric measurements

| Cross section (1/m-sr) | Vertical resolution | Horizontal resolution | Measurement accuracy (%) |
|---|---|---|---|
| $>10^{-4}$ | 75 m | 200 m | 5 |
| $10^{-4}$–$10^{-6}$ | 300 m | 10 km | 10 |
| $10^{-6}$–$10^{-7}$ | 300 m | 50 km | 20 |

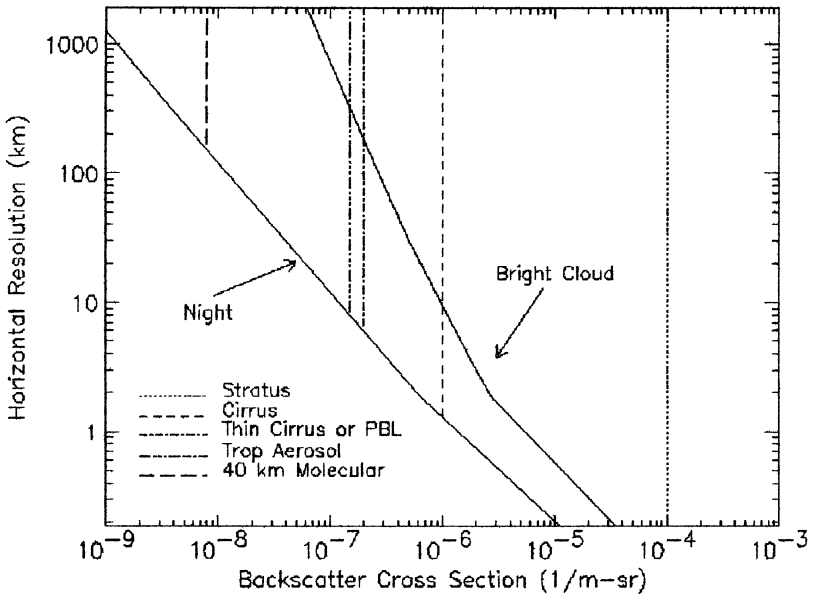


Fig. 3.2. The minimum backscatter cross section that GLAS can detect (at a signal to noise ratio of 5) as a function of horizontal resolution for nighttime and bright background conditions (solid lines). Vertical lines indicate typical backscatter cross sections for various clouds and aerosols.

Model-derived estimates of the minimum detectable backscatter cross-section as a function of the horizontal resolution (or number of shots averaged) are shown in Fig. 3.2 for nighttime and the worst expected daytime background conditions. During nighttime, GLAS is expected to resolve thin (sub-visible) cirrus layers and tenuous aerosol layers ($5\times10^{-8}$ (m-sr) $^{-1}$) at a horizontal resolution of about 50 km. Normal cirrus and denser aerosol layers ($10^{-6}$ (m-sr)$^{-1}$) will be detectable at about the 2 km resolution. Clouds with backscatter cross sections greater than about $10^{-5}$ (m-sr)$^{-1}$ will be detected on a shot to shot basis (172 m horizontal resolution). During daytime, these resolutions will vary according to the background intensity, but will generally be about 5–10 times less than the nighttime resolution. For horizontal averaging intervals less than 1000 km, the absolute minimum detectable backscatter cross section is about $10^{-7}$ and $10^{-9}$ (m-sr)$^{-1}$ during day and night, respectively.

## 4. Land and vegetation science

The Earth's surface consists of a complex mosaic of land forms and vegetative cover resulting in large variations in elevation, slope, roughness, reflectance, and vegetation height. Present day landscapes have been generated by the integrated effects of a diverse set of lithospheric, cryospheric, hydrospheric, ecologic, atmospheric, and anthroprogenic processes. Documentation of these landscape properties, and the associated dynamics, is a first step in understanding the interplay between these formative processes. Characterization of the landscape is also necessary for physical models that depend on interactions between the land and other components of the Earth system, such as predictive models of global climate change. Adequate knowledge of these

characteristics is also essential for proper utilization of the land as a resource, as well as for prediction and mitigation of natural hazards (e.g., earthquakes, volcanic eruptions, landslides, floods, wild fires).

Current physical descriptions of land properties on a global basis are in many respects inadequate. The best publicly available global representations of the Earth's topography are Digital Elevation Models (DEMs) with a spatial resolution of 1 km (Hastings and Dunbar, 1999), which are too coarse for the needs of most physical studies of land process. Moreover, these DEMs are amalgams of many disparate topographic sources, often with inconsistent or poorly known accuracies and a bewildering collection of horizontal and vertical datums. Global characterizations of land cover (e.g., Hansen et al., 2000; Loveland et al., 2000) and vegetation properties (e.g., DeFries et al., 2000) have recently been produced at moderate spatial resolution using satellite remote sensing data. Comparisons of alternative global land cover products (Hansen and Reed, 2000) reveal considerable discrepancies between the products, and there is currently no satisfactory method for validating global maps of land cover or vegetation properties. Current sensors, for example, are limited for assessing tropical deforestation.

ICESat will repeatedly sample global land topography and vegetation heights to characterize landscape properties and monitor changes in dynamic landscapes. Of particular significance is the ability to re-profile ground tracks very accurately by off-nadir pointing to specific targets of interest. In mid-latitudes ($<50^\circ$), off-nadir pointing will normally not be used to follow a prescribed ground track, so tracks on repeat cycles will vary within about 1 km. However, off-nadir pointing up to $5^\circ$ to profile specific targets might be done several times a day. At the equator, a selected location could be targeted up to 12 times during the 183-day orbit cycle, and more often at higher latitudes. After launch, potential operational limitations on pointing commands will be better defined. Potential applications include long-term monitoring of water levels of selected rivers and lakes, retreat or surge of alpine glaciers, soil erosion, changes in snow depth, inflation or deflation of volcanoes, and regional response of the lithosphere to ocean tides, changes in ice loads, and tectonic stresses. Also, the effects of natural or man-made catastrophes on topography and vegetation can be targeted. Alternatively, ICESat's precise pointing capability can be used to target slightly-offset ground tracks within a selected region to achieve a more finely resolved grid of profiles for more detailed local mapping.

ICESat elevation profiles will provide independent high-accuracy data to calibrate and validate topographic and land cover products generated by other means. In particular, high-resolution DEMs and land cover products are being derived from optical imaging and synthetic aperture radar (SAR) systems. For example, the recent Shuttle Radar Topography Mission (SRTM) will yield a 30 m horizontal-resolution DEM between $60^\circ$ N and $57^\circ$ S latitudes from interferometric SAR, and the ASTER instrument on Terra yields local DEMs of similar resolution by stereophotogrammetry. Typical vertical resolution is a few meters. However, these DEMs have inherent systematic and random errors. The ICESat elevation profiles, defined in a consistent, Earth-centered reference frame, can be used to evaluate these DEMs and establish global geodetic control, as demonstrated using profiles from the Shuttle Laser Altimeter experiment (Sun and Ranson, 1997; Garvin et al., 1998; Harding et al., 1999; and Sun et al., 2000).

Derivation of vegetation height data, and topographic profiles of the ground surface where it is covered by vegetation, depends on interpretation of the GLAS altimetry channel waveform record for each laser pulse. ICESat waveform processing (Section 7) on the ground will decom-

pose the waveforms into vertically distinct components by fitting multiple Gaussian distributions. The analysis methods were developed using waveforms acquired by the Shuttle Laser Altimeter (Carabajal et al., 1999) and the airborne Laser Vegetation Imaging Sensor (Hofton et al., 2000a). Interpretation of the resulting Gaussian fits will depend on land cover properties and local surface relief. For footprints lacking vegetation cover or cultural features, the overall centroid of the Gaussian fit is taken to be the mean surface elevation within the footprint. In the case of multiple echos, the individual Gaussians are assumed to define the elevation of discrete surfaces: for example, upper and lower flat-lying areas separated by a cliff. The width of each Gaussian contains information on the relief of the corresponding surface due to the combined effects of slope and roughness. For footprints containing vegetation and/or cultural features, surface relief effects are combined with those of the height distribution of canopy components (living or dead foliage and woody tissue) and cultural features. Where the surface relief is flat or very muted and sufficient laser energy penetrates the canopy to the underlying ground, a lowest echo is acquired in the waveform and is interpreted as originating from the ground surface. Higher echos are interpreted to correspond to vegetation layers and/or the tops of cultural features. The very first echo corresponds to the upper-most detected canopy surface or highest cultural feature. Where surface relief is pronounced, the ground, vegetation, and cultural features become unresolved in the waveform because their height distributions intermix.

The use of laser waveforms to derive vegetation height information and ground topography beneath vegetation has focused on contiguous footprints with diameters in the range 8–25 m acquired by airborne systems (Blair et al., 1999; Harding et al., 2000). Hofton et al. (2000b) describe topographic mapping of the Long Valley caldera in California, and Weishampel et al. (2000) report on canopy vertical structure mapping of a tropical rainforest in Costa Rica. Laser waveforms have been used to estimate ecologically important forest stand attributes including stem density and above-ground biomass (Lefsky et al., 1999a,b; Means et al., 1999), and the vertical distribution of plant area (Harding et al., in press) and light transmission (Parker et al., in press). Unlike the smaller, contiguous footprints of the upcoming Vegetation Canopy Lidar mission (Dubayah et al., 1997), the large, non-contiguous GLAS footprints are not optimized for retrieval of vegetation height data. Nonetheless, the GLAS waveforms will have higher vertical resolution and signal-to-noise ratios, and will provide important sampling vegetation height, especially in areas of low relief where the ground and canopy echos can be decomposed. Harding et al. (in press) computed average canopy height profiles for areas nominally $50 \times 50$ m in size, nearly the size of a GLAS footprint. These large-area height profiles reproducibly revealed variations in ecologically important canopy attributes, including maximum height, and the height, depth and relative plant area of overstory, midstory, and understory layers. In sloped or topographically rough areas, ICESat will provide information on the total within-footprint relief due to the combined vertical distributions of the ground, vegetation, and cultural features.

## 5. Sea ice and ocean science

The polar oceans are covered by a seasonally varying layer of sea ice, varying in thickness from centimeters to a few meters (e.g. Gloersen et al., 1992). Sea ice affects both the overlying atmosphere and the underlying oceans in several ways. It is a strong insulator, limiting heat exchange

between ocean and atmosphere, it modulates the exchange of momentum between atmosphere and ocean, and with its high albedo it strongly affects the absorption of radiant energy by the Earth. During formation, sea ice rejects salt, and it produces fresh water when melting, thus affecting the salinity structure of the ocean with important ramifications for deep convection, bottom-water formation, and blooms of ocean biological productivity associated with the ice edge in spring. In addition to these characteristics that influence weather and climate in ways that are still poorly understood, sea ice obstructs shipping, modifies submarine acoustics, and provides an environment essential to the survival of a wide variety of polar animals.

Sea ice is a complex material consisting of an ice matrix with inclusions of air, brine, solid salt and contaminants. It varies, spatially and temporally in thickness, composition, snow cover, wetness, and surface roughness. During the winter, the surface is generally covered by snow, which in summer may melt to form slush and melt ponds. Particularly in the Antarctic, where ice is thinner, heavy snow loads can depress the ice sufficiently to permit flooding of seawater above the ice/snow interface. Since 1972, satellite remote sensing systems have been the major tools for mapping and monitoring the sea ice, with emphasis on microwave sensors, both active and passive (e.g. Carsey, 1992; Comiso, 1995; Perovich, 1996). However, sea ice thickness and roughness are important parameters for which observation from space has been elusive.

Most sea ice can be regarded as a nearly-horizontal rough surface with ridges and hummocks, which are formed during convergence of the ice pack, and leads with open water or thin ice, which are formed during divergence of the ice pack. The roughness is an indication of the history of the ice, and strongly influences its drag coefficient and hence its response to winds in terms of turbulent energy exchanges and drag-induced flow dynamics. The sea-ice elevations will also help improve knowledge of the geoid in polar regions. The reflectance is indicative of sea-ice albedo, which also affects energy exchange. The surface elevation of flat regions is slightly higher than local sea-surface elevation, depending on the ice thickness and snow cover. Sea-ice covered ocean also contains icebergs, with surface elevations of tens to several hundred meters.

The major sea-ice parameters to be determined from GLAS ranges and waveform shapes include surface elevation, surface roughness, and reflectivity. In addition, the freeboard of icebergs will be measured wherever ICESat orbits pass over icebergs. Recent work with satellite radar-altimeter data (Peacock et al., 1998) indicates the possibility of estimating sea-ice freeboard, a proxy indicator of sea ice thickness by comparing elevations of open-water leads with those of the intervening ice. Data from GLAS could be better suited to this application, because of their small footprint and unambiguous measurement of the snow-ice surface over all types of sea ice. Even if identification of open-water waveforms is difficult, it might be possible to identify leads by the abrupt change in elevation between lead and sea ice. If successful, this capability would represent a major enhancement to our ability to monitor sea ice thickness and climatic changes.

ICESat will spend much of its time over the ocean acquiring information on sea-surface characteristics. The shape of the GLAS echo-pulse waveform will be determined primarily by the surface-height distribution within the footprint, which is small enough to be affected by individual large waves. Over distances of cm to a few hundred meters, the sea surface is roughened by waves and ocean swell, but averaged over distances of many kilometers the sea surface is almost flat. Nevertheless, surface slopes and long-wavelength undulations are present, caused by variations in Earth's gravity field, associated for instance with sea mounts, ocean currents, and variations in atmospheric pressure and seawater density. Satellite radar altimeters have shown remarkable

success in measuring sea-surface elevation and significant waveheights (e.g. Fu et al., 1994). Because of its larger pulse-limited footprint (>1.2 km) and pulse averaging, a satellite radar altimeter averages the effect of the small-scale roughness over multiple footprints typically along 300–600 m, from which estimates of surface elevation and roughness are derived. Consequently, the resulting sea-surface elevations can be used to study the longer-wavelength variability, and estimates of surface roughness are a statistical indication of the wave height.

For each GLAS echo pulse from the ocean surface, the average surface elevation and the surface-height distribution within the corresponding 60-meter footprint will be obtained. However, these footprints will, in general, cover less than one of the longer ocean waves, and it will be necessary to include information from many consecutive footprints to infer sea-surface elevation and wave height. Nevertheless, we expect GLAS to complement satellite radar-altimeter data, particularly near coastlines and islands, where the large radar beam-limited footprints include the effects of coastal topography. Moreover, details of the surface-height distribution within the laser footprints may help understand better the electro-magnetic bias errors in the radar data caused by asymmetries in the wave-height distribution and other factors.

## 6. GLAS instrument characteristics

The GLAS instrument will measure the distance to the Earth's surface with 1064 nm laser pulses and the vertical distributions of clouds and aerosols with both 1064-nm pulses and 532 nm pulses. The measurements include the strengths of the received signals and the height distributions of the reflecting surfaces. The GLAS instrument (Abshire et al., 2000) utilizes three identical diode-pumped Q-switched ND:YAG laser transmitters (Afzal et al., 2000), a 1-m diameter Beryllium receiver telescope, solid state detectors for 1064 and 532 nm signals, a subsystem to measure the pointing angle of each laser pulse, and waveform digitizers to record the laser backscatter signals at both 1064 and 532 nm. The GLAS components (Fig. 6.1) are mounted on an L-shaped optical bench and the thermal radiators are mounted at right angles on the ends of the benches. The instrument specifications are summarized in Table 6.1.

GLAS has three identical Nd:YAG laser transmitters to meet its 3-year minimum lifetime requirement. One laser will operate continuously, and alternate lasers will be turned on and optically selected via flip mirror assemblies as needed during the mission. The lasers, which are passively Q-switched, diode-pumped, and conductively-cooled, emit approximately 6-ns wide pulses in a beam with a TEMoo spatial mode. Each laser transmitter uses a Q-switched master oscillator to establish the laser pulse length and spatial beam quality, followed by two double-pass, zig-zag slab laser amplifiers that increase the pulse energy. A nonlinear optical crystal is used to convert part of the pulse energy to 532 nm. For each laser firing, the energy output from the laser is about 75 mJ is at 1064 nm and 35 mJ at 532 nm. The transmitted pulse has a divergence of approximately 110 μrad, which will illuminate a spot on the Earth's surface with a diameter of about 60 m. The laser pulses at 40 Hz rate, producing a separation of illuminated footprints on the Earth's surface of 172 m. Calculations show that the GLAS ranging error is <10 cm for clear-sky atmospheric transmissions of 50% and for surface slopes less than 5° (Fig. 6.2). The 10 s time markers from the GPS receiver provide the long-term standard for the GLAS altimeter clock frequency, which allows accurate conversion of waveform samples into time of flight.

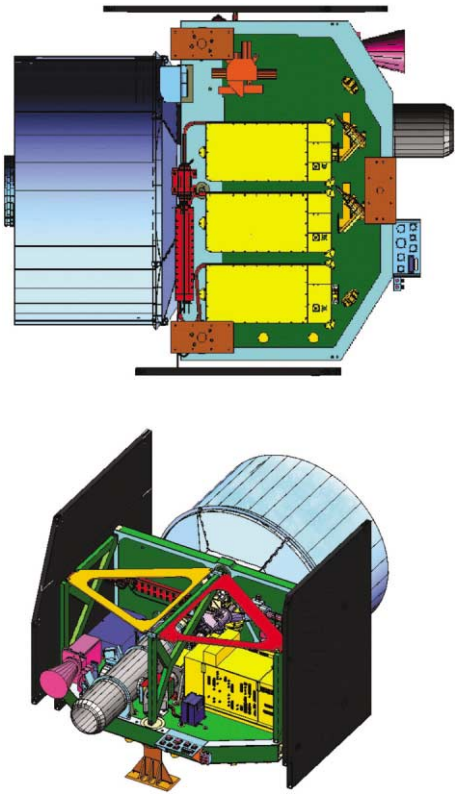

Fig. 6.1. Views of GLAS showing at top the 3 laser boxes (yellow) on the optical bench, 1-m diameter telescope with shroud, heat pipe (red), and side radiators, and at bottom the GLAS star tracker (pink), electronics boxes, and the small telescope (grey) of the stellar reference system.

The laser light backscattered from the atmosphere and Earth's surface is collected by the GLAS receiver telescope. The 1064-nm receiver has a 500 μrad field of view and an 800 pm optical bandpass and two (redundant) Si APD detectors with ~160 MHz bandwidths. The second detector can be selected if needed by a flip mirror. The 1064 nm receiver digitizes both the transmitted and backscatter signals at 1 GHz, which allows analysis of the surface echos with a time resolution of 1 ns and corresponding range resolution of 15 cm for each digitized sample. The 1064-nm signal is also separately filtered and digitized at 2 MHz for detection of dense clouds and aerosols at 76.8-m vertical resolution. Laser backscatter measurements at 532 nm are much more sensitive to weak scattering layers in the atmospheric, due to the GLAS filters, photon-counting detectors, and along-track signal integration. For the 532 nm receiver, a wide 370-pm optical prefilter and a narrow 30-pm Fabry–Perot etalon filter reject background light. The center wavelength of the solid etalon filter is thermally-tuned by a feedback loop to track variations in the 532-nm laser wavelength. The 532-nm receiver also has a narrow 170 μrad field of view and utilizes a movable mirror assembly to keep it centered on the laser signal. After passing through the etalon filter, the 532-nm signal is distributed via beam splitters to eight photon counting detectors, which operate in Geiger mode with ~60% photon-counting efficiency. Optically-thin aerosols will be detected during both day and night conditions.

Table 6.1
GLAS instrument specifications

| Laser type | ND:YAG slab, 3 stage Q-switched, diode-pumped |
|---|---|
| Number of lasers | 3 (Operate alternately) |
| Laser pulse firing rate | 40 Hz |
| Laser pulse width | 6 ns (nominal) |
| Laser energy (nominal) | 75 mJ, 1064 nm (transmitted)<br>35 mJ, 532 nm (transmitted) |
| Laser divergence angle ($1/e^2$ pts) | 70- 110 urad (depends on laser) |
| Telescope diameter | 100 cm |
| 1064 nm Detector | Si APD- analog mode (1 prime + 1 backup) |
| 1064 Surface digitizer resolution | 1 nsec (15 cm in range) |
| 1064 nm Cloud digitizer resolution | 500 nsec (75 m in range) |
| 532 nm Detector | Si APD- Geiger mode (8 used in parallel) |
| 532 nm Aerosol digitizer resolution | 500 nsec (75 m in range) |
| Laser beam angle measurement | $<10$ uradian relative to star field |
| Mass | 330 kg |
| Power | 310 W average |
| Instr. duty cycle | 100% |
| Data rate | $\sim$500 kbps (uncompressed) |
| Physical size | $\sim 110\times140\times110$ cm |
| Thermal control | Radiators with variable conductance heat pipes |

The altimeter digitizer and recorder in GLAS temporarily record the signal from the entire time-of-flight of the 1064-nm pulse to a range of 765 km from the spacecraft. This produces over 5 million digitized samples spaced at 1 ns and 15-cm range resolution. The samples are then filtered and analyzed to extract only the transmitted pulse and surface echos. The strong transmitted pulse is easy to find and extract, however the surface echos can be difficult to find due to the unknown range, pulse spreading, and possible confusing echos from cloud or haze layers. The start and end points of a search window for the surface echo are set for each pulse at the minimum and maximum possible values of the surface range, obtained to the nearest 125 m for every $1^\circ$ square on the Earth from a global-DEM file stored in GLAS. The resulting width of the search window varies from 1 km over ocean and flat terrain to 11 km over the most mountainous terrain.

A surface finding algorithm analyzes the digitized samples in the search window and extracts up to 544 sequential samples of the laser echo for transmission to the ground. The samples are first digitally filtered to maximize the probability of finding echoes from sloped or rough surfaces and to minimize the probability of selecting cloud echoes. Six digital filters are used with Gaussian impulse responses that increase in width by factors of two between filters. A separate threshold is determined for each of the filtered echos to distinguish the signal level from the noise. Each threshold is a function of the background noise, which is calculated from samples in a 1 km region that is 1 km beyond the end of the search window (i.e. below the predicted surface). Because the echo from the ground is expected to be the last local maximum in the range window, the algorithm searches in the window from below the ground upward. The response from one filter is selected by using a linear combination of weighting factors. Once a filter has been selected, the pulse location within that filtered response is used to determine the start and stop locations of the raw digitized data

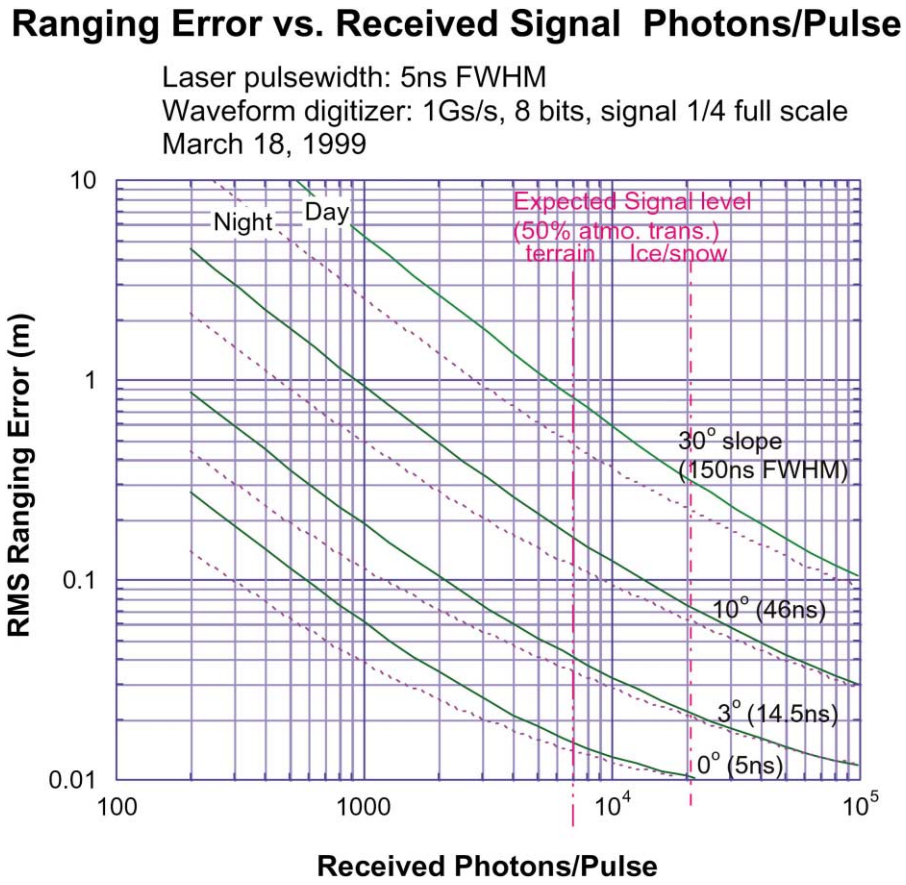


Fig. 6.2. Theoretical estimate of the GLAS ranging errors as a function of the detected photons per pulse for day (solid line) and night-time (dashed line) signal-to-noise ratios and various pulse broadenings caused by surface slopes. The expected signals for clear-sky atmospheric transmissions of 50% are 7000 photons per pulse from terrain and 20,000 photons per pulse from snow/ice surfaces. The corresponding theoretical ranging errors for 3° surface slopes are 4 cm for terrain and 2 cm for snow.

samples to transmit. Normally the first 544 of these samples over ice sheets and land (81.6 m range window) or the first 200 samples over sea ice and oceans (30 m range window) will be transmitted. Normally each sample represents 15 cm of vertical elevation. However to cover areas with larger vertical extent, the raw samples can be averaged by factors of 2, 4, or 8 before transmitting.

The atmospheric range windows are fixed at 21 km for the 1064-nm signal and 41 km for the 532-nm signal, both of which have the lower limit set at 1 km below the minimum elevation in DEM. For the upper 20 km (i.e. the stratosphere), the instrument sums forty 532-nm signals giving a 6.9 km along-track spacing (Fig. 6.3). For both channels in the 20–10 km range (upper troposphere), the instrument sums eight signals along-track for a 1.4 km along-track spacing. Below 10 km, the 40 Hz signals are retained at 172 m spacing.

The pointing angle of the centroid of each laser firing is measured relative to inertial space by the GLAS stellar reference system (SRS) to an accuracy better than 10 μrad (Sirota et al., 2000).

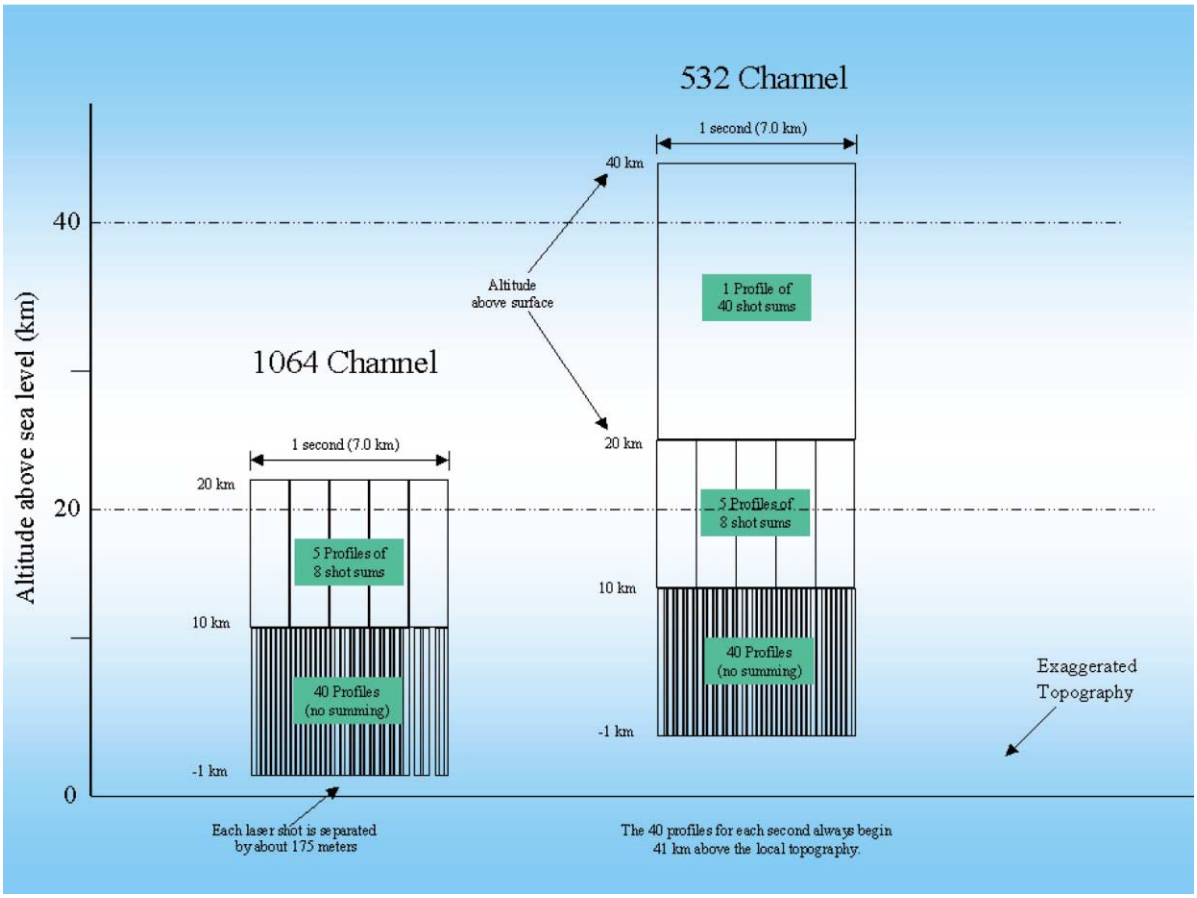


Fig. 6.3. Schematic of data collection strategy for the GLAS atmospheric channels. The laser repetition rate is 40 Hz, but the data will be summed on the spacecraft for the upper troposphere and stratosphere as indicated. The 532-nm data acquisition will extend to 41 km above the surface, but due to low signal, 1064 nm data will not be acquired above 20 km. The profiles for the 532 and 1064 channels are comprised of 548 and 280 bins, respectively, each 76.8 m wide.

The orientation of the rigid GLAS optical bench is determined relative to the star field using a zenith-viewing star-camera measurement at 10 Hz and a precision gyroscope for noise smoothing. A laser reference system (LRS) measures the orientation of each 40-Hz laser beam with respect to the same optical bench. The LRS extracts a small fraction of the outgoing laser beam into the laser reference camera (LRC) with two highly-stable cube corners. A small laser-profiling array digitizes the far-field pattern of the laser beam at 40 Hz to determine its orientation to the LRS. A CCD camera on a telescope of the LRS digitizes zenith-sky images to determine the inertial orientation of the LRS at the same 10-Hz rate as the star camera, but with a higher resolution and a narrower field-of-view. Common stars will appear in the LRC and the star camera at an average interval of 5–10 min for cross-referencing. In addition to the star tracker on the GLAS optical bench, the bus star trackers are available as a backup. Although, the mounting of the GLAS instrument to the spacecraft will distort in response to thermal variations in orbit, the distortions can be monitored and modeled.

## 7. Surface echo waveform processing

All geophysical parameters will be derived from GLAS waveform samples in ground-based data processing. The range to the mean surface within the laser footprint is determined from one-half the measured time from the transmitted pulse to the time of receipt of the echo pulse reflected from the surface, taking into account the pulse spreading (Fig. 7.1). The transmitted pulse has a distribution in time that is approximately Gaussian with a $\sigma_T$ of about 3 n. The shape of the echo waveform is affected primarily by the transmitted pulse shape, the surface height distribution within the footprint, and forward scattering in the atmosphere. As a simplification, the surface is characterized in terms of roughness and a mean slope across the footprint. Since the digitized transmitted pulse is Gaussian, the echo pulse shape will also be Gaussian, if the surface height distribution is Gaussian and atmosphere scattering effects are small. Analysis of numerous waveforms acquired by the shuttle laser altimeter has shown that most waveforms are approximated very well by a Gaussian or as a sum of Gaussians plus a noise bias. Over the oceans, sea ice, and most of the ice sheets, the echo is expected to be a single Gaussian. Over land and more complicated ice sheet regions, there may be multiple distinct surfaces within the footprint that will show up in the echo waveform as multiple distinct or overlapping Gaussian-shaped peaks. Therefore the modeled waveform is defined as

$$w(t) = e + \sum_{m=1}^{Np} A_m \exp\left[-\frac{(t - t_m)^2}{2\sigma_m^2}\right]$$

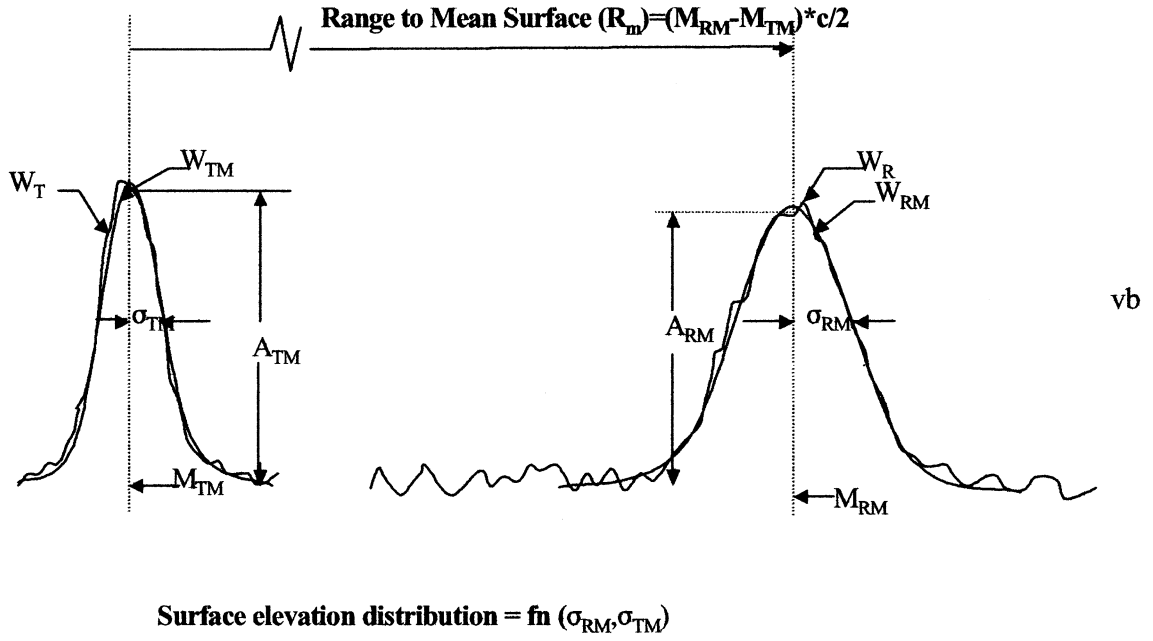


Fig. 7.1. Calculation of range and elevation distribution from typical transmitted and received GLAS pulses. *W* indicates the pulse or modeled waveform, *T* indicates the transmitted pulse, *R* indicates the received pulse, subscript *M* refers to the Gaussian model fitted to the waveform, *M* indicates the waveform mid-point, and $\sigma$ indicates the standard deviation of the waveform.

where $N_p$ is the number of peaks found in the waveform, $e$ is the bias (noise level), $A_m$ is the amplitude, $t_m$ is the temporal center, and $\sigma_m$ is the standard deviation of the $m$th Gaussian peak.

Nonlinear least squares fitting will be used to compute the model parameters in the above equation. The maximum number of peaks ($N_p$) normally calculated will be six. The range to the surface is the time between the centroid of the transmitted pulse and the center of the Gaussian fitted to the last peak of the received pulse. Because the range is calculated to the center of the fitted Gaussian, rather then to the centroid of all the data surrounding the peak, the effect of forward atmospheric scattering on the calculated range is significantly reduced. The centroid would be affected more than the central Gaussian shape, because the time delay associated with forward scattering produces an asymmetric waveform with a long tail to the right. The surface-height distribution representing the combined surface roughness and slope is calculated from the standard deviation, $\sigma_m$, of the Gaussian for the surface peak. Since it is not possible in general to separate slope and roughness, the algorithm will calculate both roughness assuming zero slope and slope assuming zero roughness.

## 8. Spacecraft and orbit characteristics

The ICESat spacecraft is a version of the commercial RS-2000 spacecraft built by Ball Aerospace in Boulder, Colorado. The RS-2000 bus, which was designed for acquiring high-resolution (1-m) commercial imagery, was first used for Quikscat launched in November 1998. The ICESat bus mass is about 670 kg and the instrument mass is about 330 kg, for a total mass of about 1000 kg. The spacecrafts orbital average power capability (5 year end of life) is 630W, in order to provide 330 W for GLAS, 216W for the bus, and a 84 W margin. The total area of the solar-panel arrays of triple junction cells is about 8 $m^2$. Although the solar panels rotate, periodic yaw maneuvers of the spacecraft are required to reorient panels with respect to the sun. The spacecraft carries instrumentation for the near-real time on-board orbit propagator and precise post-processing orbit determination. Two redundant Blackjack dual-frequency Global Positioning System receivers are connected to separate antennas mounted on the zenith deck. The receivers are similar to those on the CHAMP, GRACE and JASON missions. A unique feature is the ability to track the GPS signals on both L-band frequencies for precise positioning. The hardware and software is capable of tracking 9 or more GPS satellites. Additional orbit positioning is provided by a passive laser reflector array mounted on the nadir deck for ranging from ground-based laser systems, primarily for validation of the GPS positioning.

The spacecraft has two Ball CT-602 star trackers mounted on the zenith deck in orthogonal directions. In flight, the star-image data at 10 Hz and the gyro data from the GLAS instrument are processed in the spacecraft computer to determine the ICESat attitude autonomously for spacecraft attitude control. The agile attitude-control-system on the spacecraft allows near-nadir pointing control in normal operation and off-nadir pointing by rolling and/or pitching the spacecraft. The accuracy of the spacecraft pointing control near nadir is $\pm 10$ arcs ($1\sigma$), which is equivalent to $\pm 30$ m on the Earth. The sub-orbital track spacing will be controlled to $\pm 1$ km at the equator by periodic spacecraft thrusting (Demarest and Schutz, 2000). Based on predictions of solar flux at launch, the frequency of the maneuvers is expected to be about 5 days. At latitudes above 50° N and

S, the spacecraft will be rolled slightly to point to the reference ground tracks defined by the orbit repeat cycles to an accuracy of $\pm 35$ m ($1\sigma$) on the surface. This estimate is mainly due to errors in pointing ($\pm 35$ m) and smaller differences between the predicted and actual orbital positions between pointing-command uploads to the spacecraft. Globally, for targets of opportunity, the spacecraft can be commanded to off-nadir angles, normally limited to $\pm 5^\circ$ or about $\pm 50$ km on the surface.

The 94° orbit inclination is a compromise between the desire for true polar orbit to observe the total Antarctic ice sheet and the need for orbital crossovers for elevation change. A crossover is the intersection point on a ground track where a track ascending in latitude intersects a descending track, and would only occur at the pole in a 90° polar orbit. By differencing altimeter measurements at crossovers, common errors cancel leaving the effect of temporal change between the ascending and descending tracks plus residual errors in the measurement after corrections. To provide adequate coverage of the West Antarctic Ice Sheet, it was determined that the ground tracks should provide coverage to at least 86° S. The small uncovered area between 86° S and the South Pole will be completely enclosed by the highest density of measurements at the maximum latitude of 86° S. Occasional off-nadir pointing to the pole can be performed to provide complete elevation mapping and limited elevation change measurements to the pole. Another consideration was the geometry of the crossovers, which tend toward larger crossing angles for a 94° retrograde compared to an 86° prograde orbit. In the latitude band from 84° to 85° (North or South), the ascending and descending tracks will be approximately orthogonal.

The nominal orbit altitude of 600 km is a compromise between the GLAS instrumental preference for lower altitudes and the orbit determination and spacecraft-control preferences for higher altitude. For GLAS, the laser power needed to achieve a required signal to noise ratio of reflected light is proportional to the second power of altitude. On the other hand, a lower altitude requires more fuel for more frequent orbit adjustments to compensate for atmospheric drag. Also, the accuracy of the precision orbit determinations degrades at lower altitudes due to greater perturbations from atmospheric drag and undetermined gravity anomalies. The orbit eccentricity will be 0.0013 with a semi-major axis of about 6970 km. The position of the perigee will remain essentially fixed (“frozen orbit”) at the northernmost orbital position. Therefore, the spacecraft altitude will be primarily a function of latitude, varying between about 597 km above the ellipsoid at 86° N to 626 km above at 86° S.

The pattern of ground-tracks on the Earth will repeat with a cycle of 183-days (182.758 days and 2723 revolutions). The resulting separation between ground tracks in the same ascending or descending direction will be 14.5 km at the equator, 7 km at 60°, and 2.5 km at 80° latitude. Two sub-cycles exist within the 183-day cycle, which produce near-repeat tracks at 8-days and 25-days. The ground track pattern for 25-days will essentially repeat in the subsequent 25-days, but the pattern will be shifted westward at the equator by 14.5 km. The near-repeat 8-day pattern occurs with an eastward shift of about 100 km. The post-launch orbit will be in an 8-day repeat to enable more frequent over-flights of verification sites during the initial calibration/validation period. The day-to-day operations of ICESat will be conducted by the Laboratory for Astrophysics and Space Physics (LASP) at the University of Colorado, Boulder. LASP will be responsible for controlling the spacecraft, including the preparation of daily-command uploads, similar to their current operational control of Quikscat.

## 9. Surface elevation determination

The measured surface elevation is determined from the altitude of the satellite orbit above the Earth minus the range to the surface measured by GLAS. The range is corrected for delays caused by atmospheric refraction. Variations in the Earth's surface elevation caused by ocean, solid, atmospheric load, and polar tides are calculated to obtain the surface signals of interest. The single-pulse error budget for ICESat elevation measurements (summarized in Table 9.1) applies to ice, land and ocean/lake applications. For this error budget, it is assumed that the laser pointing error is 1.5 arcs and the surface slope is 1°. The GLAS altimeter measurement is a scalar distance measurement between a reference point in the instrument and the Earth's surface. When combined with information derived from the precision attitude determination process (PAD), the instrumentation provides an altitude vector measurement. The precision orbit determination process (POD) yields the position vector of the GLAS reference point with respect to the Earth's center of mass. By subtracting the altitude vector from the position vector of the instrument, the surface location with respect to the center of mass is calculated. The contributing factors to these vectors are dependent on various error sources, which determine the overall accuracy of the determined surface location.

The individual contributions shown in Table 9.1 are discussed in the following sections. The nature of these errors is a combination of random and systematic. The GLAS range measurement precision is characterized as random, but most of the other errors are systematic for successive pulses. However, the components of the error budget are mostly uncorrelated with each other, so the RSS of the error budget is a reasonable representation of the overall error for a single pulse. Furthermore, although some of these errors are correlated on successive pulses, the errors for a series of measurements over a given location during the life of the mission tend to be random rather than systematic. One exception to this is geographically-correlated errors in the absolute height of the orbit calculations. However, these errors can be mostly time-independent if the orbits are systematically processed with the same gravity model calculation procedures and therefore not important for elevation change measurements. Another exception is the atmospheric forward scattering (cf. Sections 3.1 and 7) if the scattering clouds have significant seasonal or interannual variations.

### 9.1. Precision orbit determination

The precision orbit determination (POD) techniques demonstrated with GPS data from TOPEX/POSEIDON (e.g., Schutz et al., 1994; Yunck, et al., 1994) will be applied to ICESat

Table 9.1
Single-shot error budget for ICESat elevation measurements

| GLAS range measurement precision | 10 cm |
|---|---|
| Radial orbit determination (POD) | 5 cm |
| Pointing determination (PAD) | 7.5 cm |
| Atmospheric delay | 2 cm |
| Atmospheric forward scattering | 2 cm |
| Other (tides, etc.) | 1 cm |
| RSS | 13.8 cm |

POD. These techniques are based on the solution of the satellite equations of motion, generally referred to as a "dynamic" approach. The GPS receiver provides measurements of pseudorange and carrier phase from the GPS satellites above the antenna ground plane. With measurements on two frequencies, ionosphere delays are removed. The few millimeter precision of the carrier phase makes it the preferred measurement for POD, even though the measurement requires resolution of an ambiguity. Two common approaches for phase measurements that solve for ambiguities with other geodetic parameters are: (1) formation of differenced measurements to remove common parameters, such a clock errors, and (2) solve for clock parameters using undifferenced measurements. In an alternate "kinematic" approach commonly used with aircraft applications the measurement geometry is used to determine position without a high-accuracy solution of the equations of motion. However, special experiments to resolve ambiguities for aircraft applications cannot be used for a satellite.

Prelaunch analysis of expected POD errors show that current gravity models can be expected to produce an error in the radial component of ICESat position that exceeds 10 cm (e.g., Rim et al., 1999). For example, EGM-96 covariance matrix predicts the error to be about 15 cm. However, experience with TOPEX/POSEIDON showed that the GPS measurements could be used to "tune" the gravity field and reduce the error contribution from this source. ICESat simulations by Rim et al. (1996, 1999) show that using ICESat GPS data can reduce the gravity errors sufficiently to reduce the radial orbit error below the 5-cm value in the error budget. In addition, ongoing efforts to improve the gravity model, combined with results from the dedicated gravity missions CHAMP and GRACE, should produce further improvements prior to and after the ICESat launch.

### *9.2. Precision attitude determination*

The precision attitude determination (PAD) process calculates the pointing of the laser beam and the position of the laser footprint on the Earth's surface. Data from the stellar-reference system (SRS) described in Section 6 will be processed to determine the GLAS laser pointing direction on a shot-by-shot basis. The instrument-star tracker (IST) mounted on the GLAS optical bench will enable determination of the orientation of the optical bench with respect to a celestial reference frame (CRF) defined by the star catalog used with the star camera images. Since the laser-profiling camera (LPC) operates at 40 Hz, an image of the far field pattern of the GLAS laser will be obtained for each pulse, so the variation of the laser direction with respect to the optical bench will be determined. Since the laser pulse is also imaged in the laser-reference camera (LRC), although at a 10 Hz rate, further monitoring of the laser direction with respect to the CRF will occur when a star appears in the LRC field of view. Simulations of the instrumentation functions and calculations, including application of a Kalman filter to the data, have shown that a 1.5 arcsec determination of laser pointing direction can be achieved (Bae and Schutz, 2000). The PAD processing will provide the laser pointing direction in the CRF, along with transformation matrices to generate the location of the illuminated laser spot in the terrestrial reference frame (TRF). The calculation of the location of the laser footprint on the surface will use the corrected GLAS range measurement and the POD and PAD outputs.

In addition to the instrumentation provided on the GLAS optical bench, the bus star trackers are available as a backup. However, the hinges used to mount the GLAS instrument to the bus can

be expected to distort in response to thermal variations experienced in orbit. These distortions will be monitored through analysis of the IST and bus tracker data. A model will be developed during the mission to predict the distortions and to improve spacecraft pointing control of the laser optical bench with respect to the Earth using the bus star trackers.

### 9.3. Atmospheric delay correction

The atmospheric delay is calculated by integrating the refractivity, as a function of pressure, temperature, and relative humidity, along the ray path (Owens, 1967). At optical wavelengths the nadir atmospheric delay is the sum of the hydrostatic delay, which is a function of surface pressure, and a residual wet delay, which is a function of total column precipitable water vapor (Quinn and Herring, 2000). For a surface pressure of 1000 mbar, the nadir hydrostatic delay is approximately 2.35 m. The precipitable water vapor contribution to delay is small, but highly variable. The conversion is approximately 0.076 mm of delay per $kg/m^2$ of precipitable water vapor. In polar regions, precipitable water vapor values are generally much less than 10 $kg/m^2$, and delay is less than 1 mm. Tropical values are as much as 50 $kg/m^2$, leading to delays of 4 mm. Similar estimates apply for off-nadir angles up to 20°.

Surface pressure is calculated using the National Center for Environmental Prediction (NCEP) 1° gridded fields of atmospheric variables. The GLAS error budget assumes less than 20 mm single-pulse atmospheric delay RMS error. Comparisons of model estimates with polar Automatic Weather Station (AWS) data in 1994 show a root-mean-squares (RMS) error of less than 5 mbar, after a mean offset is removed to correct for uncertainties in station heights. This error corresponds to delay errors of less than 12 mm. The RMS error in the calculated precipitable water vapor is less than 2 $kg/m^2$, or 0.15 mm of delay, as estimated using the technique of GPS meteorology (Quinn and Herring, 1999).

### 9.4. Tidal corrections

The basic solid Earth and ocean tide corrections required are essentially the same as those developed for radar altimetry missions, such as TOPEX-Poseidon. These corrections and the associated software are fully documented in the International Earth Rotation Service (IERS) technical notes (e.g. McCarthy, 1996). However, for the ICESat mission, ocean-load tides and tides on ice shelves are more important than for previous missions. Ocean-load tides are the secondary tidal effects on the Earth's crust caused by the variable loading of ocean tides. Ocean-load tides are largest in the continental margins and near-shore regions where GLAS will provide continuous altimetry profiles going from land to ocean. The largest ice sheet elevation changes are likely to be found near the coast. Yi et al. (2000) calculated that vertical displacements of several cm due to ocean-load tides are expected along the Antarctic margin, using the SPOTL software of Agnew (1996). However, the details of ocean tide models are most uncertain right near Antarctica, because direct radar-altimeter observations at high latitudes are scarce and the poor knowledge of bathymetry around Antarctica limits the accuracy of hydro-dynamical ocean tide models (Le Provost et al., 1995). The Antarctic ice shelves respond to tides in extremely complex ways because of the dynamic effects of water circulation inside the ocean cavity underlying the ice. In most instances the cavity geometry is poorly known, and surface data records are

very sparse. A notable exception is the Amery Ice Shelf where extensive measurements have led to the development of an accurate tide model constrained by precise GPS observations at the surface (Padman et al., 2000). ICESat data over ice shelves will need to be corrected for tidal variations to isolate non-tidal effects. In turn, ICESat will provide important new data on tides at high latitudes.

## 10. Calibration and validation

The fundamental objective of calibration/validation (CV) is to validate the science data products to ensure that appropriate geophysical interpretations can be drawn from the products. The identification and removal of non-geophysical artifacts from the data products is an important element of the CV process. The GLAS instrument will undergo extensive pre-launch testing for calibration, including experiments to characterize the dependency of the calibration parameters on environmental factors such as thermal variations. The post-launch phase of CV will verify the pre-launch parameters in flight through a variety of experiments, which are described in the following sections. In particular, the post-launch CV will assess the existence of biases in the measured altitude and pointing parameters with respect to the pre-launch values.

### *10.1. Detailed measurements over small target areas*

Small target areas will be instrumented to verify the GLAS performance and validate the various components in the error budget. The target areas on flat surfaces, such as White Sands (NM) and Bonneville Salt Flats (UT) and selected southern hemisphere sites, will be surveyed with GPS. These flat surfaces provide albedo and surface characteristics that are similar to ice sheets, but also aid the verification of the instrument measured surface elevation in the near-nadir pointing direction. The error budget given in Table 9.1 essentially applies to the verification of the altitude measurement using flat surfaces. With near-nadir pointing to a flat surface, the contribution of pointing errors to range is small (e.g., 30 arcs pointing error contributes less than 1 cm). If all corrections to the altitude measurement were known precisely, the existence of an altitude bias would be evaluated by using several measurements over the flat surface to average out the gaussian noise in the measurement. For example, 40 shots (1 s, or 7 km along-track) will reduce the 10 cm instrument precision to 1.6 cm (10 cm/40). Provided that variations in the flat surface can be characterized at a comparable level over 7 km and that other corrections can be made at a comparable level, the flat surface will enable assessment of a range bias at the few centimeter level.

To verify the performance of the pointing determination, small target areas will be instrumented to emulate a ground-based CCD camera. This emulation will be accomplished in two ways: (1) an aircraft carrying a CCD camera will image the GLAS spot on the surface with respect to ground fiducial markers and (2) ground detectors in a grid pattern will serve as a raster-device. Ground geodetic surveys using high accuracy processing techniques will provide the positions of the fiducial markers and detectors at the centimeter level in the same reference frame used for POD and PAD processing. Both approaches are being designed to support determination

of the location of the illuminated spot to an accuracy compatible with the 1.5 arcs (4.5 m) pointing knowledge requirement. Laboratory testing of the detectors with energy levels comparable to those expected for the illuminated GLAS spot has been successfully accomplished and flight tests of the airborne technique are in progress. In addition, with appropriate timing elements attached to the detectors, the time tag of the GLAS pulses will be verified to better than 1 μs.

The White Sands or Bonneville target areas will be further instrumented to validate the atmospheric delay. In addition, a ground-based lidar will enable independent characterization of the atmospheric properties during a GLAS overflight. To the extent possible, a ground-based satellite laser ranging data acquired at high-elevation angles will be used to verify the POD determination of GLAS radial position.

### *10.2. Aircraft underflights*

Aircraft flights both before and after ICESat launch are planned for detailed mapping of segments of orbit tracks over the Greenland ice sheet and nearby sea ice, over western US, over the Dry Valleys in Antarctica, and possibly over the desert in Saudi Arabia. Surface elevations will be measured along tracks ranging from 50 to 300 km long to an accuracy of 10 cm or better by NASA's Airborne Topographic Mapper (ATM) scanning laser (Krabill et al., 1995). These measurements will be compared with surface elevations and surface roughness derived from GLAS data. The surveyed segments will be sufficiently wide (approximately 300 m) to include most GLAS footprints when ICESat is pointed to the segments, and will include terrain with a range of surface slopes and roughness. The effect of ICESat pointing errors on GLAS-derived elevations will be determined by the surveyed surface slopes, and consequently should be separable from altitude errors. Thus, in addition to an overall assessment of GLAS performance, comparison between GLAS and ATM elevations will provide estimates of pointing and altitude bias at different locations around the orbit.

The prime objective of the Greenland surveys is to validate performance over both ice-sheet and sea-ice surfaces. Surveyed orbit segments will include surface types ranging from smooth, flat, and nearly horizontal to sloping and undulating ice sheet, and crevassed glaciers and rough sea ice. Some segments will pass over the narrow (few kms) Greenland outlet glaciers, with associated high albedo contrast between the dark rock margins and the glaciers. Because the ice-sheet surface elevation is expected to change with time, the Greenland ATM surveys will be made as close to simultaneous as possible (within 1 or 2 days) with ICESat passes. These flights are planned for May 2003.

Other ATM surveys will be over stable terrain (little or no elevation change over time) that can provide "benchmark" surfaces for routine GLAS validation throughout the mission. Selected surfaces are arid and largely vegetation free. Before launch, surveys will be made over several arid sites in the western US (and possibly in Saudi Arabia). Each survey will include all the183-day Mapping–Phase orbits (about 12 km apart in western US) that lie within approximately 100km X 100km, over terrain ranging from nearly flat to rough and sloping. In addition, segments of nearby 8-day post-launch phase orbits will be surveyed. An ICESat overflight of a surveyed orbit segment will occur at least twice per month. In addition, surveys of a range of vegetated sites in the northwest US will be used to assess GLAS performance over forest and woodland. GLAS

performance will be validated at different locations around the globe, primarily to ensure that there are no scaling errors associated with differing orbit heights. Consequently, we plan surveys of the ice-free areas in the Dry Valleys, near the US station in McMurdo, Antarctica, in collaboration with USGS and NSF. In addition, it may be possible to obtain surveys of parts of the Amery Ice Shelf and the Australian Desert in a collaborative effort with the Australian Antarctic Division and others.

### *10.3. Integrated residual analysis*

Comprehensive on-orbit calibration of the performance of the GLAS instrument and verification of its data products will use data analysis methods based on the techniques of integrated residual analysis as described by Rowlands et al. (2000). Residuals are formed between the observed and computed parameters in each of the three data types that constitute laser altimetry: range, pointing, and orbit. Analysis proceeds by simultaneous processing and weighting of the various data types in order to minimize residuals. In this way, all data types both contribute to the solution and are refined as systematic errors (biases) are identified and removed from the integrated solution. When GLAS observations fall on reference surfaces where the surface elevation is known at the 1–10-cm level, GLAS range data will be used to refine the pointing angle data and the ICESat orbit solution, as well as the laser range and timing biases. Reference surfaces include the open ocean, lakes, and land targets with well-characterized and stable topography. Single tracks of laser elevation profiles and cross-overs between two independent profiles over the reference surfaces are used in the analyses. Rowlands et al. (2000) describe specific forms of residual analysis including Range-Residual Analysis (RRA) and Crossover-Residual Analysis (CRA).

The basis of RRA and CRA is a Bayesian least-squares estimation and batch processing approach. A rigorous measurement model is employed in which the various parameters of laser altimeter pointing and range data, orbit tracking data, spacecraft force models, and geophysical models are simultaneously adjusted to minimize the range residuals. All significant terms that affect the 3-D location of the laser footprint on the Earth's surface are measured or modeled and described in a system of simultaneous differential equations (one for each laser observation). The equations are then solved for hundreds of unknown biases and model parameters. Typically thousands of data equations are used. The output of the parameter estimation process is a set of attitude, range, and orbit bias terms for calibration of the GLAS instrument and the attitude and orbit determinations. The methodology utilizes GEODYN, a state-of-the-art orbit determination and geodetic parameter estimation system (Pavlis et al., 1999). The RRA technique for laser altimetry was initially developed to improve the pointing, positioning, and range knowledge in the Shuttle Laser Altimeter (SLA) experiment (Garvin et al., 1998). The SLA measurements had an initial attitude uncertainty from 0.1 to 1°, because the laser pointing angle was not directly measured. Application of the RRA and CRA to SLA data processing has resulted in greater than a factor of two improvement in geolocation over the standard data product (Luthcke, this issue). A simultaneous solution of pointing, ranging and positioning parameters from a combined reduction of SLA direct altimetry and dynamic crossover data was employed in the combined RR-CRA (Luthcke, this issue). Over a factor of two improvement in SLA ocean direct altimeter range and crossover

residuals has been gained from the RRA and CRA. The resultant residuals are now dominated by ranging precision, and when smoothed to remove this noise, are at the 24 cm ($1-\sigma$) level. This remaining error is due to residual radial orbit error and remaining SSH modeling error (Luthcke et al., in press).

For ICESat, occasional roll and pitch maneuvers of the spacecraft, called ocean sweeps, will be performed to point the laser beam up to 5° off-nadir to specifically achieve sub-arc sec calibration of laser beam pointing angle biases. This calibration procedure employs the rather large sensitivity of laser range measurement to laser-beam pointing-angle (Bufton, 1989; Gardner, 1992; Harding et al., 1994) and uses range-residual analysis (RRA) with the ocean surface as reference. Open-ocean surface elevations are known from radar altimeter measurements and tidal modeling to an accuracy of 3–12 cm ($1-\sigma$) (Luthcke et al., 2000), providing a global reference surface throughout the mission. Ocean waves are not a factor due to averaging over thousands of individual laser pulses along 100 to 10,000 km ocean segments. Luthcke et al. (2000) have shown that the GLAS laser attitude can be determined to the sub-arc sec ($1-\sigma$) level from a 30 min duration (i.e. 1/3 orbit) ocean sweeps, in which the spacecraft points off nadir in a slow, conical-shaped roll and pitch maneuver up to a maximum of 5°. This simulation employed realistic, worst-case error models and included the effects of ocean surface waves and data loss from clouds. For practical considerations, ICESat's ocean sweeps will be diamond-shaped, providing most of the simulated sensitivity. Present plans call for a minimum of one ocean sweep per week, with more frequent sweeps during the initial CV period. Biases will thus be assessed as a function of temporally varying parameters, such as the orientation of the spacecraft with respect to the sun, which may thermally induce pointing variations. The ocean-sweep simulations produce a sub-5cm range bias solution simultaneously with the sub-arcsec level attitude bias determination (Luthcke et al., 2000). Applying the same measurement model as used for ocean sweeps, range-residuals will also be evaluated against Digital Elevation Models (DEMs) of stable landform surfaces obtained by airborne laser altimeter mapping.

For ICESat, the CRA is expected to provide cm-level verification of elevation differences at cross-overs and improve the estimates of range and attitude biases. As with RRA, CRA uses the GEODYN software suite. Constraint equations are formulated in terms of a minimum distance between two intersecting altimeter profiles, instead of just the height difference at a crossover point. The CRA approach was first developed to exploit the small footprint capability of laser altimetry and to take into account the simultaneous improvement in range, attitude, and orbit biases. Rowlands et al., (1999) demonstrated an order-of-magnitude improvement in the accuracy of Mars Orbiting Laser Altimeter (MOLA) geolocation using CRA.

Residuals can also be formed between the geolocated laser footprints and the 3-dimensional coordinates of land topography at reference sites having a high-resolution DEM. By differencing the GLAS elevation profiles with DEM data, the GLAS accuracy can be assessed using methods described in Rowlands et al. (2000). If the DEM has meter-level spatial resolution and significant vertical structure within a GLAS footprint, it is further possible to conduct integrated residual analysis for pulse waveforms. The time history of the laser backscatter from sloping and/or vegetated terrain is compared with a synthesized waveform for validation of footprint location and direct comparison with derived parameters (e.g. surface slope and vegetation height). This process of waveform matching is described in Rowlands et al. (2000) and Blair and Hofton (1999).

## 11. Data products and availability

The ICESat/GLAS standard data products are summarized in Table 11.1, and more detailed information is given at http://glas.wff.nasa.gov/. The 16 standard data products (GLA01 to GLA16) will be created by the ICESat Science Investigator-led Processing System (I-SIPS) at the Goddard Space Flight Center. After the initial calibration/validation period, the data will be processed and products sent within a few weeks following data collection to the National Snow and Ice Data Center (NSIDC) ECS DAAC. NSIDC will distribute data requested by the community of users. All products are time-ordered, as collected along track, and will be distributed in granules (files) as defined in the table. Metadata (time, location, quality, etc) are provided with each granule, so the metadata can be searched using NSIDC tools to determine which granules to order. Several times during the mission, the data will be reprocessed to provide improved products with improved algorithms.

Table 11.1
ICESat/GLAS standard data products

| Product ID | Granule size Mbytes | Product name GLAS/ICESat) | Primary intended users |
|---|---|---|---|
| GLA00 | 6 h | L0 Global Instrument Packet | Instrument team, ISIPS |
| GLA01 | ~1/4 orbit 34 MB | L1A Global Altimetry | ISIPS, Science team, altimeter scientists |
| GLA02 | 2 orbits 703 MB | L1A Global Atmosphere | ISIPS, Science team |
| GLA03 | 2 orbits 13 MB | L1A Global Engineering | ISIPS, Instrument team |
| GLA04 | 6 h 610 MB | L1A Global Stellar Reference and GPS | Science and Instrument teams |
| GLA05 | ~1/4 orbit 21 MB | L1B Global Waveform-based Range Corrections | ISIPS, Science team, altimeter scientists |
| GLA06 | ~1/4 orbit 9 MB | L1B Global Elevations | ISIPS, Science team, altimeter scientists |
| GLA07 | 2 orbits 828 MB | L1B Global Backscatter | ISIPS, Lidar scientists, Science team |
| GLA08 | 14 orbits 2 MB | L2 Global PBL & Elev. Aerosol Layer Heights | ISIPS, Atmospheric scientists |
| GLA09 | 14 orbits 81 MB | L2 Global Cloud Heights for Multi-layer Clouds | ISIPS, Atmospheric scientists |
| GLA10 | 14 orbits 301 MB | L2 Global Aerosol Vertical Structure | ISIPS, Atmospheric scientists |
| GLA11 | 14 orbits 12 MB | L2 Global Thin Cloud/ Aerosol Optical Depths | ISIPS, Atmospheric scientists |
| GLA12 | 14 orbits 49 MB | L2 Polar Ice Sheet Altimetry | Ice scientists |
| GLA13 | 14 orbits 22 MB | L2 Sea Ice Altimetry | Ice scientists |
| GLA14 | 14 orbits 273 MB | L2 Global Land Surface Altimetry | Land scientists and topographic mapping |
| GLA15 | 14 orbits 240 MB | L2 Ocean Altimetry | Ice and Ocean scientists |
| GLA16 | 14 orbits TBD MB | Global L3 Elevation and Atmosphere (HDF-EOS) | Multidisciplinary scientists |

The products are defined as level 0, level 1, level 2, and level 3 according to the EOS standards. Level 0 is the raw telemetry data, level 1 includes instrument parameters, and level 2 and 3 have geophysical ice, ocean, atmosphere, and land parameters. Additional level 3 and 4 products will be defined to include gridded digital elevation models and atmospheric (lidar) backscatter images. The level 1 and level 2 products are in easy-to-read integer binary format.

## 12. Summary

The ICESat mission has a broad mixture of multidisciplinary scientific objectives in glaciology, atmospheric science, climatology, and land processes, even though it carries only a single instrument. The GLAS instrument has been designed with a combination of synergistic measurement capabilities to meet the principal scientific objective of measuring small changes in the surface elevations of the polar ice sheets, while also supporting a host of other investigations. The small well-located footprint of the laser beam, with a well-defined surface reflection, will significantly improve the accuracy and coverage of satellite altimeter measurements compared to prior satellite radar altimetry. Also, the dedication of the mission to a primary scientific objective required a high-latitude orbit inclination that is optimized for ice sheet research.

The inclusion of the lidar channel in GLAS required approximately 50% higher power in the primary 1064 nm laser channel and additional detectors and electronics, while utilizing the same telescope and many other common elements of the instrument, spacecraft, and the overall mission. In return, the GLAS atmospheric measurements not only broaden the science of the ICESat mission to studies of the climatic impacts of clouds and aerosols, but will also improve the accuracy of the ice-sheet altimetry measurements. In particular, ICESat's atmospheric measurements should greatly improve our knowledge of the distribution, heights, and types of polar clouds. Previous measurements of cloud cover in polar regions have been very limited by the capabilities of spaceborne passive sensors in the polar darkness. The inadequacy of such knowledge, for example, seriously limited our ability to make accurate estimates of the percent of polar cloud cover that will obscure the GLAS primary altimeter range measurements over the ice sheets. Also, of direct importance to ice sheet science, will be improvements in our understanding of polar clouds and precipitation, which is a major determinant of the surface mass balance of the ice sheets. While GLAS could have been designed to operate only over the polar ice sheets, global operations enables measurements of land and ocean topography for significant improvements in the accuracy of land topography and a variety of applications that will develop as various investigators explore the utility of ICESat data.

Initially, the major satellites in NASA's Earth Observing System (EOS) were each planned as a series of three 5-year missions to systematically acquire global-change data sets for a period of 15 years. The first mission, Terra, was launched in December 1999 and the second mission, Aqua, was launched in May 2002. The schedules and description of these and associated missions are given at http://www.earth.nasa.gov/ along with a research strategy for follow-on missions. One category of observations is systematic measurements that are needed for long-term continuity of data on critical environmental variables inherent in global change. The NASA's research strategy notes that systematic is not necessarily synonymous with continuous measurement, but continuous measurements are required when short-term natural variability or calibration uncertainties between successive discontinuous records would mask significant long-term trends. For example, over-

lapping measurement records from successive sensors are required when no ground-based observation can provide an independent calibration standard. Although the ERS-1 and ERS-2 missions and their radar altimeters are nearly identical, their measurements over ice sheets were found to have a spatially-variant inter-satellite bias of 5–40 cm that did not occur over oceans and could not have been discovered if the mission operations had not overlapped. For ICESat, the calibration plan is intended to reduce the vulnerability to gaps in successive laser altimetry missions. More important, however, are the seasonal and interannual variability in ice sheet surface elevations and mass balance. For example, the data in Fig. 2.2 for 7 years of elevation change and Fig. 2.4 for 20 years of temperature and surface melting illustrate a well-know interannual variability in ice-sheet surface mass balance and surface climate that might preclude deductions on decadal-scale trends from records of short duration or with gaps of several years. Therefore, it is anticipated that a successful ICESat mission and follow-on polar laser-altimeter missions will parallel the ocean radar altimeter missions for monitoring significant elements of climate change contributing to global sea level rise.

## References

Abdalati, W., Steffen, K., 1997. Snowmelt on the Greenland Ice Sheet as derived from passive microwave satellite data. J. Climate 10 (2), 165–175.

Abdalati, W., Krabill, W., Frederick, E., Manizade, S., Martin, C., Sonntag, J., Swift, R., Thomas, R., Wright, W., Yungel, J. Outlet glacier and margin elevation changes: Near coastal thinning of the Greenland ice sheet. J. Geophys. Res. (in press).

Abshire, J.B., Ketchum, E.A., Afzal, R.S., Millar, P.S., Sun, X., 2000. The Geoscience Laser Altimeter System (GLAS) for the ICESat mission. In: Conference on Lasers and Electro-Optics, OSA Technical Digest. Optical Society of America, Washington, DC, pp. 602–603.

Afzal, R.S., Dallas, J.L., Yu, A.W., Mamacos, W.A., Lukemire, A., Schroder, B., Melak, A., 2000. The Geoscience Laser Altimeter System laser transmitter. In: Conference on Lasers and Electro-Optics, OSA Technical Digest. Optical Society of America, Washington, DC, pp. 50–51.

Agnew, D.C., 1996. SPOTL: some programs for ocean-tide loading. In: Scripps Institution of Oceanography Reference Series, 96–8, 35 pp.

Alley, R.B., Meese, D.A., Shuman, C.A., Gow, A.J., Taylor, K.C., Grootes, P.M., White, J.W.C., Ram, M., Waddington, E.D., Mayewski, P.A., Zielinski, G.A., 1993. Abrupt increase in Greenland snow accumulation at the end of the Younger Dryas event. Nature 362, 527–529.

Arthern, R.T., Wingham, D.J., 1998. The natural fluctuations of firn densification and their effect on the geodetic determination of ice sheet mass balance. Climate Change 40, 605–624.

Bae, S., Schutz, B., 2000. Laser pointing determination using stellar reference system in Geoscience Laser Altimeter System. In: C. Kluever et al. (Eds.), Spaceflight Mechanics 2000, Univelt Publ.

Bentley, C.R., 1997. Rapid sea-level rise soon from west antarctic ice sheet collapse? Science 275, 1077.

Bindschadler, R., 1998. Future of the West Antarctic Ice Sheet. Science 282, 428–429.

Blair, J.B., Hofton, M.A., 1999. Modeling laser altimeter return waveforms over complex vegetation using high-resolution elevation data. Geo. Res. Letters 26, 2509–2512.

Blair, J.B., Rabine, D.L., Hofton, M.A., 1999. The Laser Vegetation Imaging Sensor (LVIS): a medium-altitude, digitization-only, airborne laser altimeter for mapping vegetation and topography. ISPRS J. Photogram. Remote Sens. 54, 115–122.

Brenner, A.C., Zwally, H.J., Cornejo, H., Saba, J.L., 2000. Investigation of correlations between variations of radar backscatter with altimeter-derived ice sheet elevation changes and ERS-2/ERS-1 biases. In: Proc. ESA ERS-Envisat Symposium, ESA.

Bromwich, D.H., Chen, Q., Bai, L., Cassano, E.N., Li, Y., 2001. Modeled precipitation variability over the Greenland Ice Sheet. J. Geophy. Res. 106, D24. 33,891–33,908.

Bufton, J., 1989. Laser altimetry measurements from aircraft and spacecraft. Proc. of EEE 77, 463–477.

Campbell, W. J. et al., 1979. Report of Ice and Climate Experiment (ICEX) Science and Applications Working Group, NASA Goddard Space Flight Center.

Carsey, F. D. (Ed.), 1992. Microwave remote sensing of sea ice. American Geophysical Union, 462 pp.

Carabajal, C.C., Harding, D.J., Luthcke, S.B., Fong, W., Rowton, S.C., Frawley, J.J., 1999. Processing of shuttle laser altimeter range and return pulse data in support of SLA-02. In: Proc. ISPRS Workshop Mapping Surface Structure and Topography by Airborne and Spaceborne Lasers, La Jolla, CA. Int. Archives Photogramm. Remote Sens. 32(3W14): pp. 65–72.

Comiso, J.C., 1995. Satellite remote sensing of the Arctic ocean and adjacent seas. Arctic Oceanography: Marginal Ice Zones and Continental Shelves. Coastal and Estuarines Studies 49, 1–50.

Curran, R.J., 1989. NASA's plans to observe earth's atmosphere with Lidar. IEEE Trans. on Geosci. Remote Sens. 27 (2), 154–163.

Davis, C.H., Kluever, C.A., Haines, B.J., 1998. Elevation change of the Southern Greenland Ice Sheet. Science 279, 2086–2088.

Davis, C.H., Kluever, C.A., Haines, B.J., Perez, C., Toon, Y.T., 2000. Improved elevation change measurement of the Southern Greenland Ice Sheet from satellite altimetry. IEEE Trans. Geosci. Remote Sens. 38, 1367–1378.

DeFries, R.S., Hansen, M.C., Townsend, J.R.G., 2000. Global continuous files of vegetation characteristics: a linear mixture model applied to multi-year 8 km AVHRR data. Int. J. Rem. Sens. 21, 1389–1414.

Demarest, P., Schutz, B., 2000. An improved strategy for maintaining repeat ground tracks at high latitudes. In: C. Kluever et al. (Eds.), Spaceflight Mechanics 2000. Univelt Publ.

Douglas, B., 1997. Global sea level rise: a redetermination. Surveys of Geophysics 18 (2–3), 279–292.

Dubayah, R., Blair, J.B., Bufton, J.L., Clark, D.B., JaJa, J., Knox, R., Luthcke, S.B., Prince, S., Weishampel, J., 1997. The Vegetation Canopy Lidar mission. In: Proc. Land Satellite Information in the Next Decade II: Sources and Applications, pp. 100–112.

Duda, D.P., Spinhirne, J.D., Eloranta, E.W., 2000. Atmospheric multiple scattering effects on GLAS altimetry. Part I: calculations of single pulse bias. IEEE Trans. Geo. Rem. Sens. 39, 92–101.

Fitzharris, B.B., Allison, I., Braithwaite, R.J., Brown, J., Foehn, P.M.B., Haeberi, W., Higuchi, K., Kotlyakov, V.M., Prowse, T.D., Rinaldi, C.A., Wadhams, P., Woo, M.-K., Youyu, X., 1996. The cryosphere: changes and their impacts. In: Climate Change 1995, Impacts, Adaptations and Mitigation of Climate Change: Scientific-Technical Analyses. Cambridge University Press, Cambridge, chapter 7, 878 pp.

Fu, L.I., Christensen, E.J., Yamarone, C.A. et-al., 1994. TOPEX/Poseidon Mission Overview. J GEOPHYS Res.-Oceans 99 (C12), 24369–24381.

Gardner, C., 1992. S, Ranging performance of satellite laser altimeters. IEEE Trans. on Geoscience and Remote Sensing 30, 1061–1072.

Garvin, J., Bufton, J., Blair, J., Harding, D., Luthcke, S., Frawley, J., Rowlands, D., 1998. Observations of the Earth's topography from the Shuttle Laser Altimeter (SLA): laser-pulse echo-recovery measurements of terrestrial surfaces. Phys. Chem. Earth 23, 1053–1068.

Hastings, D., Dunbar, P.K., 1999. The Global Land One-kilometer Base Elevation (GLOBE) Digital Elevation Model, NGDC Key to Geophysical Records Documentation No. 34, National Oceanic and Atmospheric Administration, National Geophysical Data Center, 325 Broadway, Boulder, Colorado 80303, USA.

Gloersen, P., Campbell, W.J., Comiso, J.C., Cavalieri, D.J., Parkinson, C.L., Zwally, H.J., 1992. Arctic and Antarctic Sea Ice 1978–1987: Satellite Passive Microwave Observations and Analysis, NASA SP-511, 290 p.

Hansen, M.C., Reed, B., 2000. A comparison of the IGBP DISCover and University of Maryland 1 km global land cover products. Int. J. Rem. Sens. 21, 2000. 1365–1373.

Hansen, M.C., DeFries, R.S., Townshend, J.R.G., Sohlberg, R., 2000. Global land cover classification at 1 km spatial resolution using a classification tree approach. Int. J. Rem. Sens. 21, 1331–1364.

Harding, D.J., Bufton, J.L., Frawley, J.J., 1994. Satellite laser altimetry of terrestrial topography; vertical accuracy as a function of surface slope, roughness, and cloud cover. IEEE Trans. Geosci. Rem. Sens. 32, 329–339.

Harding, D.J., Gesch, D.B. Carabajal, C.C., Luthcke, S.B., 1999. Application of the Shuttle Laser Altimeter in an

Accuracy Assessment of GTOPO30, a Global 1-Kilometer Digital Elevation Model. In: Proc. ISPRS Workshop Mapping Surface Structure and Topography by Airborne and Spaceborne Lasers, La Jolla, CA. Int. Archives Photogram. Rem. Sens. 32(3-W14), pp. 81–85.

Harding, D.J., Blair, J.B., Rabine, D.L., Still, K.L., 2000. SLICER Airborne laser altimeter characterization of canopy structure and sub-canopy topography for the BOREAS northern and southern study regions: instrument and data product description. In: Hall, F., Nickeson, J. (Eds.), Technical Report Series on the Boreal Ecosystem-Atmosphere Study (BOREAS): Remote Sensing Sciences Group. NASA/TM-2000–209891.

Harding, D.J., Lefsky, M.A., Parker, G.G., Blair, J.B. Laser altimeter canopy height profiles: methods and validation for deciduous, broadleaf forests. Rem. Sens. Environ. (in press).

Hofton, M.A., Minster, J.B., Blair, J.B., 2000a. Decomposition of laser altimeter waveforms. IEEE Trans. Geosci. Remote Sens. 38, 1989–1996.

Hofton, M.A., Blair, J.B., Minster, J.B., Ridgway, J.R., Williams, N.P., Bufton, J.L., Rabine, D.L., 2000b. An airborne scanning laser altimetry survey of Long Valley, California. Int. J. Remote Sens. 21, 2413–2437.

Houghton, J. T., Callander, B. A, Varney, S. K., 1992. The 1992 IPCC supplement: scientific assessment. In: Climate Change 1992: The Supplementary Report to the IPCC Scientific Assessment. Cambridge University Press, Cambridge.

Huybrechts, P., Le Muer, E., 1999. Predicted present-day evolution patterns of ice thickness and bedrock elevation over Greenland and Antarctica. Polar Research 18 (2), 299–306.

Jensen, E.J., Toon, O.B., Selkirk, H.B., Spinhirne, J.D., 1996. On the formation and persistence of subvisible cirrus clouds near the tropical tropopause. J. Geophs. Res. 101 (21), 361–375.

Krabill, W.B., Thomas, R.H., Martin, C.F., Swift, R.N., Frederick, E.B., 1995. Accuracy of airborne laser altimetry over the Greenland ice sheet. Int. J. Remote Sens. 16, 1211–1222.

Krabill, W., Abdalati, W., Frederick, E., Manizade, S., Martin, C., Sonntag, J., Swift, R., Thomas, R., Wright, W., Yungel, J., 2000. Greenland Ice Sheet: high-elevation balance and peripheral thinning. Science 289, 428–430.

Le Provost, C., Bennett, A.F., Cartwright, D.E., 1995. Ocean tides for and from TOPEX/Poseidon. Science 267, 639–642.

Lefsky, M.A., Harding, D.J., Cohen, W.B., Parker, G.G., Shugart, H.H., 1999a. Lidar remote sensing of forest basal area and biomass: application and theory. Remote Sens. Environ. 67, 83–98.

Lefsky, M., Cohen, W., Acker, S., Parker, G., Spies, T., Harding, D., 1999b. Lidar remote sensing of biophysical properties and canopy structure of forests of Douglas-fir and western hemlock. Remote Sens. Environ. 70, 339–361.

Loveland, T.R., Reed, B.C., Brown, J.F., Ohlen, D.O., Zhu, Z., Yang, L., Merchant, J.W., 2000. Development of a global land cover characteristics database and IGBP DISCover from 1 km AVHRR data. Int. J. Rem. Sens. 21, 1303–1330.

Luthcke, S.B., Rowlands, D.D., McCarthy, J.J., Pavlis, D.E., Stoneking, E., 2000. Spaceborne laser altimeter.i pointing bias calibration from range residual analysis. J. Spacecraft Roc. 37, 374–384.

Luthcke, S. B., Carabajal, C.C., Rowlands, D.D., Enhanced geolocation of spaceborne laser altimeter surface returns: parameter calibration from the simultaneous reduction of altimeter range and navigation tracking data, J. Geodynamics, this issue.

McCarthy, D.D. (Ed), 1996. IERS Standards. In: IERS Technical Note 21, Observatoire de Paris.

Means, J.E., Acker, S.A., Harding, D.J., Blair, J.B., Lefsky, M.J., Cohen, W.B., Harmon, M.E., Mckee, W.A., 1999. Use of large-footprint scanning airborne lidar to estimate forest stand characteristics in the western Cascades of Oregon. Remote Sens. Environ. 67, 298–308.

National Academy of Science, 1990. Sea-Level Change. National Academy Press, Washington, DC.

Nerem, R.S., Haines, B.J., Hendricks, J. et-al., 1997. Improved determination of global mean sea level variations using TOPEX/Poseidon altimeter data. Geophys J. Res. Lett. 24 (11), 1331–1334.

Neumann, J.E., Yohe, G., Nicholls, R., 2000. Sea-level rise and global climate change: a review of impacts to U.S. coasts. In: Pew Center on Global Climate Change. Arlington, VA, 38 pp.

Oppenheimer, M., 1998. Global warming and the stability of the West Antarctic Ice Sheet. Nature 393, 325–332.

Owens, J.C., 1967. Optical refractive index of air: dependence on pressure, temperature, and composition. Appl. Opt. 6, 51–59.

Padman, L., Fricker, H.A., Coleman, R., 2000. An inverse tide model for the Antarctic ice shelves and seas. EOS, Trans. Am. Geophys. U.

Palm, S.P., Hagan, D., Schwemmer, G., Melfi, S.H., 1998. Inference of marine atmospheric boundary layer moisture and temperature structure using airborne Lidar and infrared radiometer data. J. Appl. Meteor. 37, 308–324.

Parker, G.G., Lefsky, M.A., Harding, D.J. Light transmittance in forest canopies determined using airborne laser altimetry and in-canopy quantum measurements. Remote Sens. Environ. (in press).

Pavlis D.E., Moore D., Luo S., McCarthy J.J., Luthcke S.B., 1999. GEODYN Operations Manual: 5 Vols. Raytheon ITSS, Greenbelt, MD.

Peacock, N.R., Laxon, S.W., Scharoo, R., Maslowski, W., Winebrenner, D.P., 1998. Geophysical signatures from precise altimetric height measurements in the Arctic Ocean. In: Proc. Intl. Geosci. Rem. Sens. Symp., Seattle, pp. 1964–1966.

Perovich, D.K., 1996. The optical properties of sea ice. In: CRREL Monograph 96–1, US Army Corps of Engineers CRREL, 24 pp.

Quinn, K.J., Herring, T.A., 1999. Using the global GPS network to validate atmospheric delay corrections to the ICESat laser altimeter ranges. EOS Trans. AGU 79 (Suppl.), 200.

Quinn, K.J., Herring, T.A., 2000. Atmospheric delay correction to GLAS laser altimeter ranges. In: GLAS Algorithm Theoretical Basis Document.

Rignot, E., 1998. Fast recession of a West Antarctic glacier. Science 281, 549–551.

Rim, H., Davis, G., Schutz, B., 1996. Dynamic orbit determination for the EOS laser altimeter satellite (EOS ALT/GLAS) using GPS measurements. J. Astronautical Sci. 44 (3), 409–424.

Rim, H., Web, C., Schutz, B., 1999. Analysis of GPS and satellite laser ranging (SLR) data for ICESat precision orbit determination. Paper AAS-99–146, AAS/AIAA Space Flight Mechanics Meeting.

Rossow, W.B., Cairns, B., 1995. Monitoring Changes of Clouds. Climatic Change 31, 301–347.

Rowlands, D.D., Pavlis, D.E., Lemoine, F.G., Nuemann, G.A., Luthcke, S.B., 1999. The use of laser altimetry in the orbit and attitude determination of Mars Global Surveyor. Geo. Res. Letters 26, 1191–1194.

Rowlands, D.D., Carabajal, C.C., Luthcke, S.B., Harding, D.J., Sauber, J.M., Bufton, J.L., 2000. Satellite laser altimetry: on-orbit calibration techniques for precise geolocation. Rev. Laser Eng. 28.

Schutz, B., Tapley, B., Abusali, P., Rim, H., 1994. Dynamic orbit determination using GPS measurements from TOPEX/Poseidon. Geophys. Res. Letters 21 (19), 2179–2182.

Sirota, J.M., Millar, P.S., Volodin, B., Brown, T., March, J., Bae, S., 2000. Inertially referenced laser pointing determination system. In: Conference on Lasers and Electro-Optics, OSA Technical Digest. Optical Society of America, Washington, DC, pp. 603–604.

Spinhirne, J.D., Palm, S.P., 1996. Space based atmospheric measurements by GLAS. In: Ansmann, A. (Ed.), Advances in Atmospheric Remote Sensing with Lidar. Springer, Berlin, pp. 213–217.

Sun, G., Ranson, K.J., 1997. Digital elevation models from SIR-C interferometric and Shuttle Laser Altimeter (SLA) data. In: Proc. IGARSS'97, Singapore, pp. 460–462.

Sun, G., Ranson, K.J., Bufton, J., Roth, M., 2000. Requirement of ground tie points for InSAR DEM generation. Photogram. Eng. Rem. Sens. 66, 81–85.

Thomas, R., Csatho, B., Fahnestock, M., Gogineni, P., Kim, C., Sonntag, J., 2000a. Mass balance of the Greenland Ice Sheet at high elevations. Science 289, 5478. 426–427.

Thomas, R.H., Abdalati, W., Akins, T.L., Csatho, B.M., Frederick, E.B., Gogineni, S.P., Krabill, W.B., Manizade, S.S., Rignot, E.J., 2000b. Substantial thinning of a major east Greenland outlet glacier. Geophys. Res. Lett. 27 (9), 1291–1294.

Trenberth, K. E., Houghton, J. T., Meira Filho, L. G., 1996. The climate system: an overview. In: Climate Change 1995: The Science of Climate. Cambridge University Press, Cambridge (chapter 1).

Vaughan, D.G., Smith, A.M., Corr, H.F.J., Jenkins, A., Bentley, C.R., Stenoien, M.D., Jacobs, S.S., Kellogg, T.B., Rignot, E., Lucchitta, B.K., 2001. A review of Pine Island Glacier, West Antarctica: hypotheses of instability vs. observations of change. The West Antarctic Ice Sheet: Behavior and Environment. AGU Antarctic Research Series 77, 237–256.

Wahr, J., Wingham, D., Bentley, C., 2000. A method of combining ICESat and grace satellite data to constrain antarctic mass balance. J. Geophys. Res. 105 (B7), 16. 279–294.

Warrick, R., Le Provost, C., Meier, M., Oerlemans, J., Woodworth, P., 1996. Changes in sea level. In: Houghton, J.T. et al. (Eds.), Climate Change: The Science of Climate Change. Cambridge University Press, Cambridge, p. 572.

Weishampel, J.F., Blair, J.B., Knox, R.G., Dubayah, R., Clark, D.B., 2000. Volumetric lidar return patterns from an old-growth tropical rainforest canopy. Int. J. Remote Sens 21, 409–415.

Wingham, D.J., Ridout, A.J., Scharroo, R., Arthern, R.J., Shum, C.K., 1998. Antarctic elevation change from 1992 to 1996. Science 282.

Yi, D., Minster, J.B., Bentley, C.R., 2000. The effect of ocean tidal loading on satellite altimetry over Antarctica. Antarctic Science 12, 119–124.

Yohe, G., Schlesinger, M., 1998. Sea-level change: The expected economic cost of protection or abandonment in the United States. Climate Change 38, 447–472.

Yunck, T., Bertiger, W., Wu, S., Bar-Sever, Y., Christensen, E., Haines, B., Lichten, S., Muellerschoen, R., Vigue, Y., Willis, P., 1994. First assessment of GPS-based reduced dynamic orbit determination on TOPEX/Poseidon. Geophys. Res. Letters V 21 (7), 541–544.

Zwally, H.J., 1975. Comment. J. Glaciol. 15, 244.

Zwally, H.J., 1989. Growth of the Greenland Ice Sheet: interpretation. Science 246, 1589–1591.

Zwally, H.J., Fiegles, S.L., 1994. Extent and duration of Antarctic surface melting. J. Glaciol. 40, 136. 463–476.

Zwally, H.J., Brenner, A.C., 2001. Ice sheet dynamics and mass balance. Fu, L.-L., Cazenave, A. (Eds.), Satellite Altimetry and Earth Sciences. Academic Press, pp. 351–369.

Zwally, H.J., Jun, Li., 2002. Seasonal and interannual variations of firn densification and ice-sheet surface elevation at the Greenland summit. J. Glaciol. 48, 161.